European Journal of Cell Biology 101 (2022) 151255

Contents lists available at ScienceDirect

European Journal of Cell Biology

journal homepage: www.elsevier.com/locate/ejcb

A mechanistic protrusive-based model for 3D cell migration

Francisco Merino-Casallo [a,b,1], Maria Jose Gomez-Benito [a,b,2], Ruben Martinez-Cantin [c,d,3], Jose Manuel Garcia-Aznar [a,b,*,4]

[a] Multiscale in Mechanical and Biological Engineering (M2BE), Aragon Institute of Engineering Research (I3A), Zaragoza 50018, Spain
[b] Department of Mechanical Engineering, Universidad de Zaragoza, Zaragoza 50009, Spain
[c] Robotics, Perception and Real Time Group (RoPeRT), Aragon Institute of Engineering Research (I3A), Zaragoza 50018, Spain
[d] Department of Computer Science and System Engineering, Universidad de Zaragoza, Zaragoza 50009, Spain

ARTICLE INFO

Keywords:
3D cell migration
Protrusion dynamics
Cell mechanics
Cell - matrix interactions
Matrix mechanics
Matrix remodeling

ABSTRACT

Cell migration is essential for a variety of biological processes, such as embryogenesis, wound healing, and the immune response. After more than a century of research—mainly on flat surfaces—, there are still many unknowns about cell motility. In particular, regarding how cells migrate within 3D matrices, which more accurately replicate *in vivo* conditions. We present a novel *in silico* model of 3D mesenchymal cell migration regulated by the chemical and mechanical profile of the surrounding environment. This *in silico* model considers cell's adhesive and nuclear phenotypes, the effects of the steric hindrance of the matrix, and cells ability to degradate the ECM. These factors are crucial when investigating the increasing difficulty that migrating cells find to squeeze their nuclei through dense matrices, which may act as physical barriers. Our results agree with previous *in vitro* observations where fibroblasts cultured in collagen-based hydrogels did not durotax toward regions with higher collagen concentrations. Instead, they exhibited an adurotactic behavior, following a more random trajectory. Overall, cell's migratory response in 3D domains depends on its phenotype, and the properties of the surrounding environment, that is, 3D cell motion is strongly dependent on the context.

1. Introduction

Cell migration regulates the development and maintenance of multicellular organisms. Indeed, forming new tissues and organs during embryogenesis requires elaborate migratory patterns. During angiogenesis, endothelial cells migrate from pre-existing blood vessels to form new ones. Wound healing calls for the coordinated migration of several cell types, such as fibroblasts and epidermal cells. Cell migration is also associated with many diseases such as cancer, in which tumoral cells invade their surrounding tissue and other parts of the body during metastasis. Therefore, a comprehensive understanding of cell motility is crucial.

Cell migration is an extremely complex phenomenon involving many different biological processes and players (Merino-Casallo et al., 2022). The specific cellular context—in particular, the cell phenotype and the properties of the surrounding microenvironment—determines if and how cells migrate (Shellard and Mayor, 2020; De Pascalis and Etienne-Manneville, 2017; Friedl and Mayor, 2017; Lintz et al., 2017; Mak et al., 2016; Haeger et al., 2015). Besides, distinct external cues may bias cells' trajectory and speed. These external signals span from chemicals (e.g., gradients of soluble or surface-bound factors) to mechanical ones, such as the extracellular matrix (ECM) architecture and stiffness. Nonetheless, how cells sense these external cues, adapt, and respond by establishing a specific migratory pattern is not fully understood yet.

Cell motion has been a subject of study for more than a century (Pfeffer, 1884; Caton, 1870; Addison, 1842). The focus of the research community has been primarily on how cells migrate on two-dimensional

Abbreviations: 1D, One-Dimensional; 2D, Two-Dimensional; 3D, Three-Dimensional; ECM, Extracellular Matrix; FA, Focal Adhesion; MMP, Matrix Metalloproteinases; PI3K, Phosphoinositide 3-kinases; PM, Plasma Membrane; ROI, Region of Interest.

* Corresponding author at: Corresponding author.
E-mail address: jmgaraz@unizar.es (J.M. Garcia-Aznar).
[1] 0000–0003-3852–0987
[2] 0000–0002-1878–8997
[3] 0000–0002-6741–844X
[4] 0000–0002-9864–7683

https://doi.org/10.1016/j.ejcb.2022.151255
Received 20 January 2022; Received in revised form 15 June 2022; Accepted 1 July 2022
Available online 8 July 2022

(2D) domains until recently. Studying migratory cells on flat surfaces has considerably increased our understanding of cell migration. Still, cell behavior on plated cultures does not accurately replicate how cells behave in three-dimensional (3D) *in vivo* conditions (Chiu et al., 2014; Wu et al., 2018; Zhu et al., 2018).

In such relevant settings, a variety of cell types can switch from one mode of migration to another based on their context (Paul et al., 2019; Wang et al., 2019; Yamada and Sixt, 2019). Factors such as cell confinement, low adhesion, increased cellular contractility, and inhibited proteolytic activity promote lobopodial and amoeboid migration. Conversely, the main features of mesenchymal migration are prominent protrusions, high ECM adhesion, and proteolytic tissue remodeling.

The wide variety of actors, biological processes, and factors regulating cell migration calls for an integrative approach to unravel such complex phenomena (Buttenschön and Edelstein-Keshet, 2020; Lee et al., 2020; Movilla et al., 2019). Mathematical models have become a powerful tool to get valuable insights more efficiently. Simulators can also isolate specific mechanisms and behavior patterns more easily than their *in vitro* counterparts. Furthermore, *in silico* models may have a guiding role for experimental research by making predictions to test in the lab.

Over the last several decades, researchers have proposed many different computational models to increase our understanding of cell migration. Most of these theoretical models replicate cell motion on flat surfaces (Fang et al., 2020; Rens and Merks, 2020; Vargas et al., 2020; Zmurchok et al., 2020; Zheng et al., 2020). Nonetheless, an increasing number of mathematical models focus on cell motility within more realistic 3D microenvironments (Campbell and Bagchi, 2020; Moreira-Soares et al., 2020; Lee et al., 2020; Sun et al., 2019). Different *in silico* models have tried to mimic the distinct modes of cell migration: individual (Hervas-Raluy et al., 2019; Hoehme and Drasdo, 2010; Schlüter et al., 2012) or collective (Alert and Trepat, 2020; Escribano et al., 2018; Camley and Rappel, 2017; Letort et al., 2019), amoeboid (Campbell and Bagchi, 2017; Lim et al., 2013; Moure and Gomez, 2018), mesenchymal (Heck et al., 2020; Kim et al., 2018; Ribeiro et al., 2017), or even lobopodial (Serrano-Alcalde et al., 2020). Researchers usually focus on just one of the mechanisms involved in the migratory process (e.g., the biochemical (Hatakeyama et al., 2003; Singh et al., 2012; Wang et al., 2009), or the biophysical (Borau et al., 2011; Escribano et al., 2019; Li et al., 2019)). A few models even integrate a couple of them, such as the biochemical and biophysical mechanisms (Letort et al., 2019; Marin-Riera et al., 2016; Sun and Zaman, 2017). These models usually adopt one of the following modeling approaches: (i) discrete (Bentley et al., 2009; Scianna et al., 2012; Van Liedekerke et al., 2015), (ii) continuum (Serrano-Alcalde et al., 2017; Valero et al., 2014; Vermolen and Javierre, 2012) or (iii) hybrid (Daub and Merks, 2013; Gonzalez-Valverde and Garcia-Aznar, 2018; Milde et al., 2014). We would like to highlight the theoretical work of Kim and colleagues (2018), in which the authors defined a method to assess the ECM stiffness sensed by filopodia. The authors applied this method to model filopodial mechanosensing that resulted in guided cell migration within 3D environments.

The present work aimed to improve our knowledge of how and to what extent cell mechanics and ECM degradation regulate mesenchymal-like cell motility within 3D matrices. We created a new model that more accurately represents how the mechanical properties of cells and their surroundings influence their migratory patterns. By integrating biochemical and biomechanical stimuli, we could more accurately mimic how individual cells migrate through 3D dense microenvironments. In particular, our focus in this work was on cell-ECM interactions—which are deemed essential for mesenchymal migration. As a result, we could replicate how cells interact with their surroundings to sense external cues and modify their local microenvironment accordingly.

In the following sections, we will describe the different components of the proposed *in silico* model: from a simplified version of the chemosensing mechanism to the building blocks of the mechanism associated with cell-matrix interactions. In particular, we will emphasize how we modeled (i) protrusion dynamics, (ii) the ECM regulatory role on protrusion growth and retraction, (iii) how cells push their nucleus forward during mesenchymal migration taking into account the cell's nuclear phenotype, (iv) the formation and disassembly of cell-matrix adhesions considering the cell's adhesive phenotype, and (v) ECM degradation. Then, we will give a specific application for the proposed model. Next, we will highlight the main migratory behaviors predicted by this *in silico* model. Finally, we will give an overview of the presented model, its strengths and limitations, as well as the novelty and relevance of this work.

2. Methods

In this section, we will start by describing an *in silico* model of 3D mesenchymal cell migration that extends the proposed multi-scale model from Merino-Casallo and colleagues (2018) and Ribeiro and colleagues (2017). We will present the mathematical definition and implementation of this multi-scale model. Then, we will illustrate the application of this *in silico* model, demonstrating the predictive capabilities by comparing the numerical results with experimental data.

2.1. Model description

Here, we start by describing the main aspects of this extended multi-scale model to better understand the novel modeling enhancements proposed. This model was built upon the assumption that the mesenchymal cell migration can be described as a three-stage process (Sen-Gupta et al., 2021; Ribeiro et al., 2017). First, the cell probes its surroundings for external cues such as gradients of chemoattractant through a variety of transmembrane receptors. Secondly, when these transmembrane receptors get activated by binding to such ligands, they initiate a cascade of signaling pathways that modulate the cellular migratory response. In particular, these signaling pathways regulate the dynamics of dendritic protrusions (Senju and Lappalainen, 2019; Caswell and Zech, 2018; Svitkina, 2018; Lehtimaki et al., 2017). Finally, these protrusive structures push and pull the ECM, allowing the cell to migrate throughout the ECM. Here, we established a relationship between the contractile forces exerted by these protrusions and the cell nucleus translocation.

The proposed model simulating mesenchymal cell migration within 3D matrices was built upon some of our previous works (Merino-Casallo et al., 2018; Ribeiro et al., 2017). However, we included several novel aspects to more accurately replicate the cell, the surrounding environment, and the interactions between each other. We will start by introducing the different building blocks of the proposed model of mesenchymal-like motility within dense environments. First, we will briefly describe the chemosensing mechanism that establishes protrusions locations and their stress-free (unconstrained) length variation. Secondly, we will present the ECM model that allowed us to consider the matrix as a heterogeneous entity. Next, we will describe how we modeled protrusions expansion and contraction, which enables the nucleus translocation through ECM pores. We will also explain how this *in silico* model can consider cell's adhesive and nuclear phenotypes. Then, we will define a model of matrix degradation that allows cells to enlarge narrow ECM pores. Lastly, we will give an overview of the numerical implementation of the proposed *in silico* model and an example of its application.

2.1.1. Modeling cell behavior

We maintained the cell 3D structure proposed in our previous works (Merino-Casallo et al., 2018; Ribeiro et al., 2017). which simulated the cell body as a set of one-dimensional (1D) deformable bars joined in a centroid (Fig. 1 (right)). This centroid represented the cell nucleus. These 1D bars were located in a 3D domain and simulated protrusions

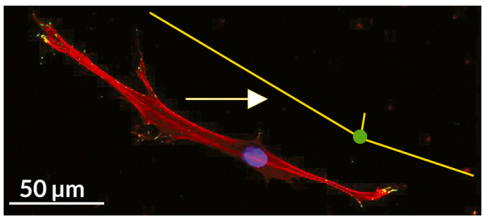

Fig. 1. Cell 3D structure scheme. **(left)** Normal Human Dermal Fibroblast (NHDF) cultured in a 4 mg/ml collagen gel, stained for actin (red), vinculin (green), and nucleus (blue). Image were captured with a confocal microscope. **(right)** *In silico* model of a mesenchymal cell migrating within 3D matrices. Protrusions are considered as 1D deformable bars (yellow), and are all linked together in a central node representing the cell nucleus (green). (Adapted from Pérez-Rodríguez and colleagues (2018)).

defining the cell body.

2.2. Chemosensing mechanism

The chemosensing mechanism enables cells to probe for biochemical cues in their surrounding ECM. The activation and deactivation of transmembrane receptors (e.g., RTKs, GPCRs) allow cells to perceive the biochemical profile of the ECM. These receptors embedded in the plasma membrane (PM) become activated by binding to different chemoattractant molecules (e.g., growth factors). When bound together, the activated receptors can activate downstream signaling molecules (e.g., phosphoinositide 3-kinases [PI3K]) located at the cytosol. As a result, the signal received in the PM is propagated inside the cell, regulating different cellular dynamics, including those of actin-based protrusions.

The spatiotemporal distribution of activated PI3K ($PI3K_A$) is closely related to protrusions dynamics and migratory patterns (Ridley et al., 2003; Petrie et al., 2009; Weiger et al., 2010; Welf et al., 2012). Therefore, we modeled a simplified signaling network (Fig. 2a). We were interested in the locations where (i) cytosolic PI3K was preferentially activated and (ii) $PI3K_A$ accumulated through time inside the cell. These features defined protrusions locations and directly influenced their expansion and contraction (Fig. 2b).

We represented the PM of the cell as a spherical surface with a fixed radius (Fig. 2b). The center of this sphere was the central node linking all protrusions in the proposed mechanical model (see Fig. 4 and Fig. 5).

More details on this chemosensing mechanism and the proposed signaling network are included in the Supplementary Section S1.

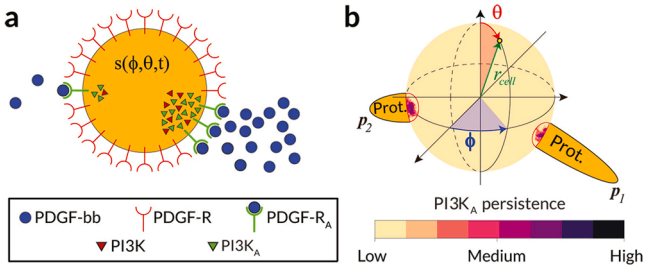

Fig. 2. Cell signaling model scheme. **a**: Two-dimensional representation of the modeled 3D chemosensing mechanism based on a simplified signaling pathway in which PDGF molecules activated their associated surface receptors (PDGFR) by binding to them. These activated PDGFR ($PDGFR_A$), in turn, activated messenger molecules of PI3K located in the cytosol. The spatial persistence of $PI3K_A$ ($s(\phi, \theta, t)$) has a regulatory role in protrusion dynamics. **b**: Scheme of the regulatory role of $PI3K_A$ persistence in protrusion dynamics. The location of $s(\phi, \theta, t)$ peaks determined protrusions location (p_1 at $[\phi_{p_1}, \theta_{p_1}]$ and p_2 at $[\phi_{p_2}, \theta_{p_2}]$), while the signal variation ($\partial s(\phi, \theta, t)/\partial t$) influences protrusions stress-free (unconstrained) length variation.

2.3. Modeling the heterogeneous behavior of the ECM

In previous works (Merino-Casallo et al., 2018; Ribeiro et al., 2017), we considered the ECM as a continuous and homogeneous entity. Nevertheless, this approximation is far from reality. The ECM internal structure builds upon a network of collagen fibers, which are interconnected by crosslinkers (Fig. 3) (Olivares et al., 2019; Theocharis et al., 2016). Still, the composition and microarchitecture of the ECM associated with each tissue are unique (Guimarães et al., 2020; Faraj et al., 2007). Further, local variations in the biophysical properties of the matrix can dramatically impact different biological processes, including cell migration (Hayn et al., 2020). Indeed, cells can sense the local properties of their surrounding ECM, such as porosity, fiber alignment, and stiffness, and adapt their behavior accordingly (Nasello et al., 2020; Taufalele et al., 2019).

Thus, modeling physiological processes such as cell migration requires a good approximation of the ECM inhomogeneities.

A realistic model of how cells' local environment influences cell migration requires considering the ECM a heterogeneous entity. Accordingly, we decided to discretize the extracellular domain in a set of voxels of a fixed size. This ECM representation allows to locally evaluate the biophysical properties of the cells' surrounding environment. Substrate stiffness influences some of the leading players in the cell-matrix interactive mechanism, such as actin (de)polymerization and actomyosin motors (Ringer et al., 2017; Rubashkin et al., 2014). Because of the ECM fibrillar interconnectivity, integrin-containing focal adhesions (FAs) allow cells to sense the stiffness of their local microenvironment (Conway and Jacquemet, 2019; Kechagia et al., 2019). We assumed that the stiffness sensed by the cell through FAs is the stiffness of the ECM surrounding those adhesion complexes. The stiffness of the ECM is another factor regulating the protrusive stretch characteristics. Therefore, in this work, we paid special attention to the ECM stiffness.

To assess the local stiffness of ECM subdomains in our biophysical model, we used simple geometric elements. One or several of these elements made up what we called regions of interest (ROI). We opted for sphere-like elements with radius r_{ROI}.

We assumed a relationship between the porosity of the matrix and its stiffness, which may change based on the physical profile of the ECM. For collagen-based hydrogels, such relationship means that as the collagen concentration increases, so does its stiffness (Valero et al., 2018). In contrast, the porosity of the matrix decreases (Zanotelli et al., 2022; Olivares et al., 2019; Fraley et al., 2015).

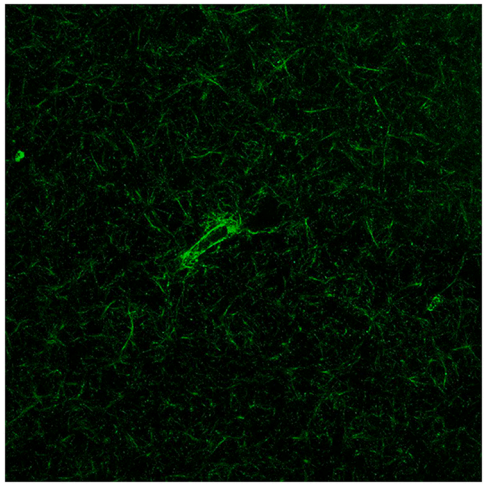

Fig. 3. Confocal image in real-time of a Primary Human Osteoblast seeded in DQ-collagen I (green fluorescence) mixed with collagen I. Image reproduced with permission from Movilla (2021).

2.4. Protrusions growth

2.4.1. Modeling cell mechanics during protrusion growth

In 3D microenvironments, actin polymerization contributes to protrusions formation and growth (Kelkar et al., 2020; Caswell and Zech, 2018). Actin polymerization occurs much more rapidly at the barbed end of actin filaments, which most of the time points toward the PM. By polymerizing against the PM, actin filaments push this membrane and the surrounding ECM.

We defined a mechanical system based on nodes and elements (bars and springs) to simulate such expansive event. Unlike our previous works (Merino-Casallo et al., 2018; Ribeiro et al., 2017), protrusions were considered as unidimensional elastic bars (p_i). The contact between these deformable bars and the surrounding matrix was simulated by means of springs. Conversely, the cell nucleus was considered the central node that connected all these elastic bars (Fig. 4). The LINC complex connects the cell nucleus to the cytoskeleton, embedding it in a meshwork that can resist high compressive loads. Therefore, the displacements of the central node (the cell nucleus) were impeded. We located nodes at the tip of the protrusions and the cell nucleus (yellow circles in Fig. 4).

We assigned a fixed rigidity to the 1D elastic bars. In contrast, the stiffness associated with the springs were calculated evaluating the rigidity of the surrounding ECM. Specifically, we assessed the rigidity of the ROIs associated with the areas that protrusions would traverse based on s_{p_i} (ROI^{exp}; Fig. 4a, green and pink rectangles).

2.4.2. Location and unconstrained length variation

We assumed the persistence of activated actin-binding regulators such as PI3K ($PI3K_A$) in the outer region of the cytosol (just below the cell surface) determines the protrusions location and their stress-free (unconstrained) length variation during their expansion. In locations where activated PI3K persistence increased, the corresponding i-th protrusion grew larger during the expansive stage. As a result, the stress-free (unconstrained) expansion of protrusions depended on signal variations of $PI3K_A$ (s) at those locations (s_{p_i}). Therefore, we computed the stress-free (unconstrained) length variation of each protrusion during its expansion based on these signal variations as:

$$\left.\frac{\partial L^f_{p_i}(s_{p_i},t)}{\partial t}\right|_{exp} = \begin{cases} \left.\frac{\partial L^f_{p_i}(s_{p_i},t)}{\partial t}\right|_{birth} & \text{if } p_i \text{ is new prot.} \\ \left.\frac{\partial L^f_{p_i}(s_{p_i},t)}{\partial t}\right|_{growth} & \text{otherwise} \end{cases}, \quad (1)$$

where s_{p_i} is the spatiotemporal variation of $PI3K_A$ associated to the i-th

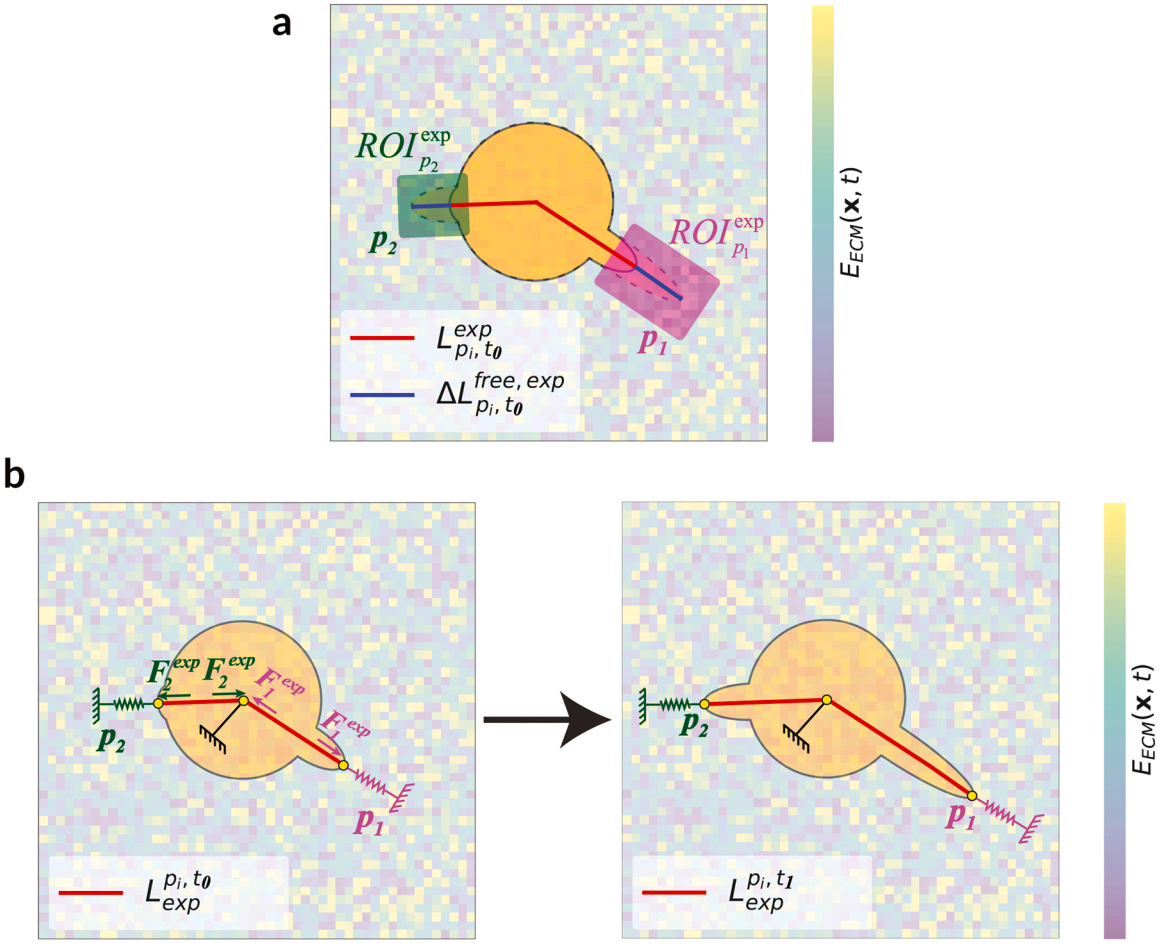

Fig. 4. Two-dimensional representation of the 3D structure associated with protrusions expansion. Two protrusions, p_1 and p_2, are represented as unidimensional elastic bars, with a fixed rigidity. The cell nucleus is the central point connecting the bars, which represent cell's protrusions. We locate a node (yellow circles) at the location of the cell nucleus and at the tip of each protrusion. The contact between these deformable bars and the surrounding matrix was simulated by means of springs. **a**: The stiffness of these springs was computed as the averaged Young's modulus of the corresponding region of interest ($ROI^{exp}_{p_1}$ and $ROI^{exp}_{p_2}$). **b**: By binding cell nucleus to the cytoskeleton, the LINC complex embeds it in a meshwork that can resist high compressive loads. Therefore, the displacements of the central node were impeded. Next, we applied forces to the nodes to simulate protrusions expansion because of actin polymerization (**left**). Finally, we computed the displacements of each node (**right**). Note that only the nodes located at the protrusions tip would move.

protrusion, $\frac{\partial L^f_{p_i}(s_{p_i},t)}{\partial t}|_{birth}$ represents the stress-free (unconstrained) length variation of the i-th protrusion during its birth (defined in Supplementary Equation S4), and $\frac{\partial L^f_{p_i}(s_{p_i},t)}{\partial t}|_{growth}$ is the stress-free (unconstrained) length variation of the i-th protrusion during its growth and stabilization (defined in Supplementary Equation S5).

More details on how we established protrusions locations and their free expansion are included in the Supplementary Section S2.

2.4.3. Simulating protrusion growth by actin polymerization

To simulate protrusions expansion because of actin polymerization, we applied forces to the aforementioned nodes located at both ends of protrusions (Fig. 4b, left). The time variation of these forces was defined as:

$$\frac{\partial \boldsymbol{F}^{exp}_{p_i}(t)}{\partial t} = \frac{E_{p_i}A}{L^{exp}_{p_i}(s_{p_i},t_0)} \frac{\partial L^f_{p_i}(s_{p_i},t)}{\partial t}|_{exp} \boldsymbol{e}_i, \quad (2)$$

where E_{p_i} represents the stiffness of the i-th protrusion, A is the area of the protrusion cross section, and $L^{exp}_{p_i}(s_{p_i},t_0)$ represents the length of the i-th protrusion at the beginning of its expansive stage (t_0). $\frac{\partial L^f_{p_i}(s_{p_i},t)}{\partial t}|_{exp}$ is the stress-free (unconstrained) length variation of the i-th protrusion during its expansion (defined in Equation 1). Lastly, $\boldsymbol{e}_i$ is the unit vector in the direction of the longitudinal axis of the i-th protrusion.

Next, we computed the displacements of each node ($\boldsymbol{u}^i(t)$; Fig. 4b, right). We took into account the stiffness of the ECM surrounding the cell and the forces generated by protrusion's expansion. The length and relative position of each protrusion were updated using these computed

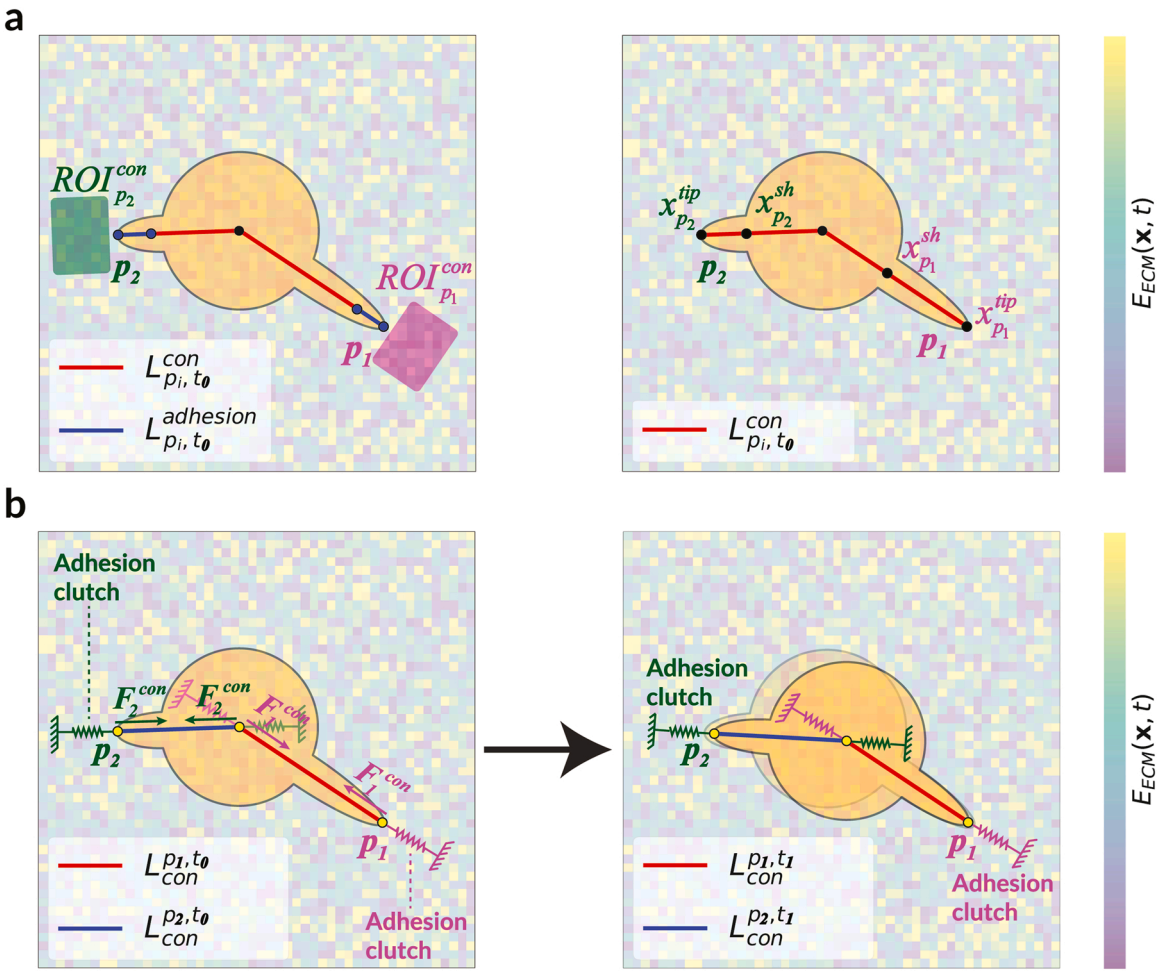

Fig. 5. Two-dimensional representation of the 3D structure associated with protrusions contraction. Two protrusions, p_1 and p_2, are represented as unidimensional elastic bars, with a fixed rigidity. The cell nucleus is the central point connecting the bars, which represent cell's protrusions. We located a node (yellow circles) at the location of the cell nucleus and at the tip of each protrusion. Their adhesive region—which allows cells to probe the surroundings through focal adhesions—was modeled as a spring. **a**: The stiffness of these springs was computed as the averaged Young's modulus of the corresponding region of interest ($ROI^{con}_{p_1}$ and $ROI^{con}_{p_2}$; **left**). During contraction, the ROIs did not overlap the space occupied by the cell's protrusions. Instead, they were located in front of them. This is where the ECM would received the maximum mechanical stimulus because of protrusions' contractions. To compute the friction term (μ) associated with the contractile force of each protrusion ($F^{con}_{p_i}(t)$), we assessed the averaged Young's modulus around the shaft of the corresponding protrusion ($x^{sh}_{p_i}$; **right**). Conversely, to compute the reaction forces ($R_{p_i}(t)$) associated with each protrusion, we evaluated the average Young's modulus around the tip of the corresponding protrusion ($x^{tip}_{p_i}$). **b**: We included adhesive clutches on FAs, which would determine protrusions adhesiveness to the surrounding ECM. We considered each protrusion connected to the cell nucleus through the cytoskeleton (and the LINC complex) as an isolated mechanical entity. Therefore, we solved the system associated with each mechanical entity independently. Each of these systems included a different spring connected to the central node, as the cell nucleus would move through a different region of the polarized cell's cytoplasm. We assumed that the stiffness of this region of the cytoplasm depended on the rigidity of the matrix around the adhesive region of each protrusion. We also assumed that the cell nucleus displacements happen in the same direction as one of the cell's protrusions. Next, we applied forces to the nodes to simulate protrusions contraction because of actin depolymerization and actomyosin motors (**left**). Finally, we computed the displacements of each node (**right**). The leading protrusion determining the cell trajectory was the one generating higher reaction forces.

displacements. Note that, as the displacements of the central node were impeded, only the nodes located at the protrusions tip would move.

2.5. Protrusions contraction

2.5.1. Modeling cell mechanics during protrusions contraction

Actin depolymerization and actomyosin motors play a key role in protrusions contraction. Actin depolymerization occurs much more rapidly at the pointed end of actin filaments, which most of the time faces inside, away from the PM. Actomyosin motors generate traction forces in the cytoskeleton, which are then transmitted to the cell nucleus by the LINC complex.

We defined a mechanical system based on nodes and elements (bars and springs) to simulate these contractile events. Protrusions were considered as unidimensional elastic bars (p_i), whereas FAs coupling the PM to the surrounding ECM were simulated by means of springs. The cell nucleus was considered the central node that connected all these elastic bars (Fig. 5). We located nodes at the tip of the protrusions and the cell nucleus (yellow circles in Fig. 5).

We assigned a fixed rigidity to the 1D elastic bars (the same rigidity than during the expansive stage). The stiffness associated with the springs were calculated evaluating the rigidity of the surrounding ECM. However, this time we assessed the rigidity of the ROIs associated with the protrusions adhesive regions (ROI^{con}; Fig. 5A, green and pink rectangles). This adhesive region had a maximum length of 8 μm (in agreement with the 8 μm–16 μm range from Wolf and colleagues (2007)).

2.5.2. Unconstrained length variation

We assumed the protrusions length at the beginning of its contractile stage determines their stress-free (unconstrained) length variation during their contraction. Therefore, we defined the stress-free (unconstrained) length variation of each protrusion during its contraction accordingly (see Supplementary Equation S6).

More details on how we established protrusion free contraction are included in the Supplementary Section S2.

2.5.3. Simulating protrusion retraction by actin depolymerization and actomyosin motors

To simulate protrusions contraction because of actin depolymerization and actomyosin motors, we applied forces to the aforementioned nodes (Fig. 5b, left). The time variation of these contractile forces were defined as:

$$\frac{\partial \boldsymbol{F}_{p_i}^{con}(t)}{\partial t} = (1-\mu)\frac{E_{p_i}A}{L_{p_i}^{con}(s_{p_i},t_0)}\frac{\partial L_{p_i}^{f}(s_{p_i},t)}{\partial t}\Big|_{con}\boldsymbol{e}_i, \tag{3}$$

where μ is a friction term (defined below, in Equation 4) enabling us to consider cell's nuclear phenotype. E_{p_i} represents the stiffness of the i-th protrusion, and A is the area of the protrusion cross section. $L_{p_i}^{con}(s_{p_i},t_0)$ is the length of the i-th protrusion at the beginning of its contractile stage (t_0). $\frac{\partial L_{p_i}^{f}(s_{p_i},t)}{\partial t}|_{con}$ represents the stress-free (unconstrained) length variation of the i-th protrusion during its contraction (defined in Supplementary Equation S6). Lastly, e_i is the unit vector in the direction of the longitudinal axis of the i-th protrusion.

Including a friction term (μ) enabled our model to replicate the increasing difficulty that cells find to migrate within dense 3D environment because of the steric hindrance effect of the ECM. We computed this friction term (μ) by means of a phenomenological law that takes into account the drag that suffers the cell nucleus through ECM pores as:

$$\mu = \begin{cases} 0 & \text{if } E_{ECM}\left(\boldsymbol{x}_{p_i}^{sh},t\right) < E_{ECM}^{no\ eff} \\ 1 & \text{if } E_{ECM}^{arrest} < E_{ECM}\left(\boldsymbol{x}_{p_i}^{sh},t\right) \\ \left(\dfrac{E_{ECM}\left(\boldsymbol{x}_{p_i}^{sh},t\right) - E_{ECM}^{no\ eff}}{E_{ECM}^{arrest} - E_{ECM}^{no\ eff}}\right)^{\gamma^{fr}} & \text{otherwise} \end{cases}, \tag{4}$$

where $E_{ECM}(\boldsymbol{x}_{p_i}^{sh},t)$ is the ECM rigidity around the i-th protrusion shaft ($\boldsymbol{x}_{p_i}^{sh}$, the ECM region through which the nucleus would be squeezed). $E_{ECM}^{no\ eff}$ is the maximum matrix stiffness allowing cells to migrate effortlessly through the ECM, that is, there is no steric hindrance effect from the matrix ($\mu = 0$). Conversely, E_{ECM}^{arrest} represents the minimum matrix stiffness resulting in a complete migration arrest because of cells inability to squeeze their nuclei through such pores ($\mu = 1$). This may occur because of the nucleus rigidity and diameter, or the pore size. Lastly, γ^{fr} is a friction coefficient. If $E_{ECM}(\boldsymbol{x}_{p_i}^{sh},t)$ is between these two boundaries, the matrix would hinder, to some extent, cell migration ($0 < \mu < 1$). Note that this friction term (μ) changes based on both the average stiffness of the ECM around the protrusion shaft ($E_{ECM}(\boldsymbol{x}_{p_i}^{sh},t)$) and the parameters $E_{ECM}^{no\ eff}$, E_{ECM}^{arrest}, and γ^{fr}. See Supplementary Section S3 for some examples, based on the proposed definition of the nuclear phenotype.

We assumed a relationship between the porosity of the matrix and its stiffness, which may change based on the physical profile of the ECM. In particular, for collagen-based hydrogels, we assumed an inverse relationship because, as the collagen concentration increases, so does its stiffness (Valero et al., 2018). Conversely, the porosity of the matrix decreases (Zanotelli et al., 2022; Olivares et al., 2019; Fraley et al., 2015). Hence, we established a couple of rigidity thresholds $E_{ECM}^{no\ eff}$ and E_{ECM}^{arrest}, which are cell type-specific and may also change based on the physical profile of the ECM. Not only because cell types may exhibit a nucleus of a different size but also because nuclear deformability may change based on factors such as the matrix composition, which would modulate cell's nuclear lamin A/C ratio or induce chromatin decompaction. For example, inhibiting lamin A/C phosphorylation in HT-1080 fibrosarcoma cells increased their nuclei stiffness (Mukherjee et al., 2020). Conversely, confined conditions in 3D induce chromatin decompaction and seem to decrease nuclear stiffness (Fischer et al., 2020, Wang et al., 2018). Therefore, this friction term (μ) would depend on cell's nuclear phenotype.

Protrusions adhered to denser and more confined regions of the ECM, with higher ECM stiffness, would have to exert higher contractile forces to squeeze cells nuclei through. This friction term (μ) would act as a penalty term, biasing the migratory toward those regions that facilitate the translocation of cells nuclei through larger pores. Still, in some scenarios, this friction term may be negligible (even zero), that is, there might be no penalty for any region of the defined ECM. Indeed, in these scenarios, cells may exhibit highly deformable or small-enough nuclei to traverse ECM pores effortlessly. The biophysical properties of the matrix may not hinder cell migration through steric hindrance either.

In this work, we focused on NHDF cells migrating in collagen-based hydrogels, so we calibrated these rigidity thresholds ($E_{ECM}^{no\ eff}$ and E_{ECM}^{arrest}) accordingly. When the stiffness of the ECM around the i-th protrusion shaft ($E_{ECM}(\boldsymbol{x}_{p_i}^{sh},t)$) is greater than $E_{ECM}^{no\ eff}$, cell's nuclear phenotype would enable cells to migrate through such pores effortlessly (Wolf et al., 2013). Otherwise, the nuclear rigidity or diameter would require cells to squeeze their nuclei to overcome the physical barrier that represents such small pores (Calero-Cuenca et al., 2018; Krause and Wolf, 2015). Still, if the stiffness of the ECM around the i-th protrusion shaft ($E_{ECM}(\boldsymbol{x}_{p_i}^{sh},t)$) is greater than E_{ECM}^{arrest}, cell's nuclear phenotype would make impossible for cells to migrate through such a confined environment,

resulting in a migratory arrest. By including γ^{fr} as a friction coefficient, we allow for a nonlinear response, which may be required to replicate the effect of the ECM steric hindrance (Insall, 2021). Note that γ^{fr} may be equal to 1, which would translate into a linear response for the ECM steric hindrance.

Next, we computed the displacements of each node ($\boldsymbol{u}^i(t)$; yellow circles in Fig. 5b, right). Again, we took into account the stiffness of the ECM surrounding the cell and the forces generated by actomyosin motors. The cell nucleus was assumed to move through the cytoplasm of the cell. During the translocation of the cell nucleus, this organelle finds opposition from the cytoskeleton. Several authors have suggested that cells cortical stiffness depends on the rigidity of the surrounding ECM (Rianna and Radmacher, 2017; Liu et al., 2013; Chopra et al., 2011; Tee et al., 2011; Solon et al., 2007). Therefore, we considered that the stiffness of this region of the cytoplasm depended on the rigidity of the matrix around the protrusions adhesive area. The length and relative position of each protrusion were updated using these computed displacements. However, based on experimental observations, we assumed that the cell nucleus displacements happen in the same direction as one of the cell's protrusions. We hypothesized cells would find lower opposition to push their nucleus forward through its cytoplasm than through the surrounding ECM. Thus, the position of the cell nucleus was determined by projecting the associated computed displacement over the direction vector of the nearest protrusion.

During mesenchymal-like migration, a leading protrusion determines cells' trajectories (Doyle et al., 2021). This leading protrusion is the one generating a higher deformation over the surrounding environment during the contractile stage. Consequently, we considered each protrusive structure connected to the cell nucleus through the cytoskeleton as an isolated mechanical entity. We solved the mechanical system associated to each protrusion and the cell nucleus individually. Then, we were able to determine the leading protrusion, that is, the one generating higher reaction forces—which we computed as:

$$\boldsymbol{R}_{p_i}(t) = \frac{E_{ECM}\left(\boldsymbol{x}_{p_i}^{tip}, t\right)A}{L_{p_i}^{con,adh}(t_1)}\boldsymbol{u}_{p_i}(t), \tag{5}$$

where $E_{ECM}(\boldsymbol{x}_{p_i}^{tip}, t)$ is the matrix rigidity around the i-th protrusion tip, A is the area of the protrusion cross section, $L_{p_i}^{adh}(t)$ is the length of the adhesive region of the i-th protrusion at the end of the contractile stage (t_1), and $\boldsymbol{u}_{p_i}(t)$ is the displacement vector of the i-th protrusion front.

Actomyosin force generation coordinates FA formation, reinforcement, and disassembly (Mason et al., 2019). Hence, on the contractile stage of our model, we also included a simplified clutch model to simulate cell-matrix adhesions (Elosegui-Artola et al., 2018; Bangasser et al., 2017) (Fig. 5b). Regarding cell-ECM interactions, forces are transmitted only if molecular bonds establish a connection between: (i) ECM and integrins, and (ii) integrins and actin cytoskeleton. These bonds must be engaged to transmit contractile reaction forces generated by myosin motors located at the base of the protrusion to the surrounding ECM (Equation 6). Protrusions exerting contractile reaction forces too low or too high detach from the ECM. The bonds connecting the integrins to the ECM fibers, and integrins to the actin cytoskeleton, play an essential role here. Contractile reaction forces must be high enough for these bonds to be engaged. However, if those forces are too high, bonds linking integrins to the surrounding matrix will break. The contractile reaction forces that determined if the i-th protrusive node (located at the tip of the i-th protrusion, see Fig. 5) was attached to the surrounding ECM was defined as:

$$p_i^{\text{attached}}(t) = \begin{cases} True & \text{if } R_{min} < \| \boldsymbol{R}_{p_i}(t) \| < R_{max} \\ False & \text{otherwise} \end{cases}, \tag{6}$$

where R_{min} and R_{max} are the lower and upper boundaries. If contractile reaction forces applied to the nodes located at the extremes of the 1D deformable bar associated to the i-th protrusion were smaller than R_{min} or bigger than R_{max}, then the corresponding bonds would not be engaged. We considered that only protrusions attached to the surrounding matrix could lead cell's migration. We also assumed that protrusions detached from the ECM retracted and subsequently disappeared. As a result, this *in silico* model could consider cell's adhesive phenotype.

2.6. ECM degradation

In dense 3D environments, cells switch to a mesenchymal-like migration based on protrusive and remodeling dynamics to overcome extracellular barriers that could, otherwise, impede cell migration (Krause et al., 2019; Yamada and Sixt, 2019). Cells generate tube-like geometries as they migrate through the ECM (Li et al., 2020). First, cell protrusions modify the ECM structure while expanding and contracting. Secondly, the cell body creates channel-like tracks while migrating through dense 3D environments (Beunk et al., 2022; Paul et al., 2017). Cells also cleave ECM collagen fibers by matrix metalloproteinases (MMPs) proteolytic activity. Even though MMPs are located all over the PM, the protrusive surface seems to have two differentiated subdomains—adhesive and proteolytic (Wolf et al., 2007). The former is located at the protrusive tip allowing cells to attach to the ECM, the latter along the shaft where ECM degradation occurs (Fig. 6). Because of this proteolytic activity, ECM porosity increases—and ECM stiffness decreases accordingly—in the regions occupied by the cell and those nearby.

The stiffness variation on location $\boldsymbol{x}$ of the ECM domain because of degradation at time t was computed as:

$$\begin{aligned} \frac{\partial E_{ECM}(\boldsymbol{x},t)}{\partial t} &= \begin{cases} -E_{ECM}(\boldsymbol{x},t) + E_{ECM}^{void} & \text{if } dist(\boldsymbol{x},\boldsymbol{x}_{cs}) \le r \\ 0 & \text{if } r' < dist(\boldsymbol{x},\boldsymbol{x}_{cs}) \\ -cl_{PM}(\boldsymbol{x})v_{deg}(\boldsymbol{x},t) & \text{otherwise} \end{cases}, \\ cl_{PM}(\boldsymbol{x}) &= 1 - \frac{dist(\boldsymbol{x},\boldsymbol{x}_{pm})}{\delta_{deg}}, \\ v_{deg}(\boldsymbol{x},t) &= \alpha_{deg}\left(\frac{E_{ECM}(\boldsymbol{x},t)}{E_{\mu}^{hydrogel}}\right), \end{aligned} \tag{7}$$

where $dist(x, x_{cs})$ is the distance from location x to the cell skeleton (x_{cs}). Whenever x is closer to one of the cell's protrusions, r represents the radius of the protrusions section ($r_{prot.} = 3.5$ μm). Conversely, when x is closer to the central region of the cell (represented as a sphere), r is the radius of this central region ($r_{cell} = 25$ μm, based on experimental observations). $r'(= r + \delta_{deg})$ delimits the ECM subdomain around the PM—where degradation occurs by MMPs proteolytic activity. We assumed a fixed δ_{deg}. We considered that locations occupied by the cell are matrix voids forming channel-like tracks. Therefore, the stiffness of these matrix voids was very low ($E_{ECM}^{void} << 1$ Pa). $E_{ECM}(x, t)$ is the stiffness in location x at time t. $cl_{PM}(x)$ assesses how close location x is from the PM ($cl_{PM}(x) = 0$, if x is at the PM whereas $cl_{PM}(x) = 1$, if x is at the frontier of the proteolytic subdomain). $v_{deg}(x, t)$ determines the cell's degradation speed. $E_{\mu}^{hydrogel}$ represents the averaged stiffness of the microenvironment assessed by Valero and colleagues (2018) based on the collagen concentration of the hydrogel where cells are embedded, and α_{deg} is a parameter regulating the MMPs cleave ratio. Matrix porosity increased—and ECM stiffness decreased accordingly—in those regions around the PM because of cells' proteolytic activity. Note that the stiffness of ECM locations in the proteolytic region ($r < d(\boldsymbol{x},\boldsymbol{x}_{cs}) \le r'$) did not decrease uniformly. Instead, the stiffness decreased more rapidly the closer these locations were to the PM (where MMPs locate) because of a diffusive phenomenon. The morphology of the cell body changed because of protrusions expansion and contraction. Hence, we updated the stiffness of the matrix surrounding the cell after computing the

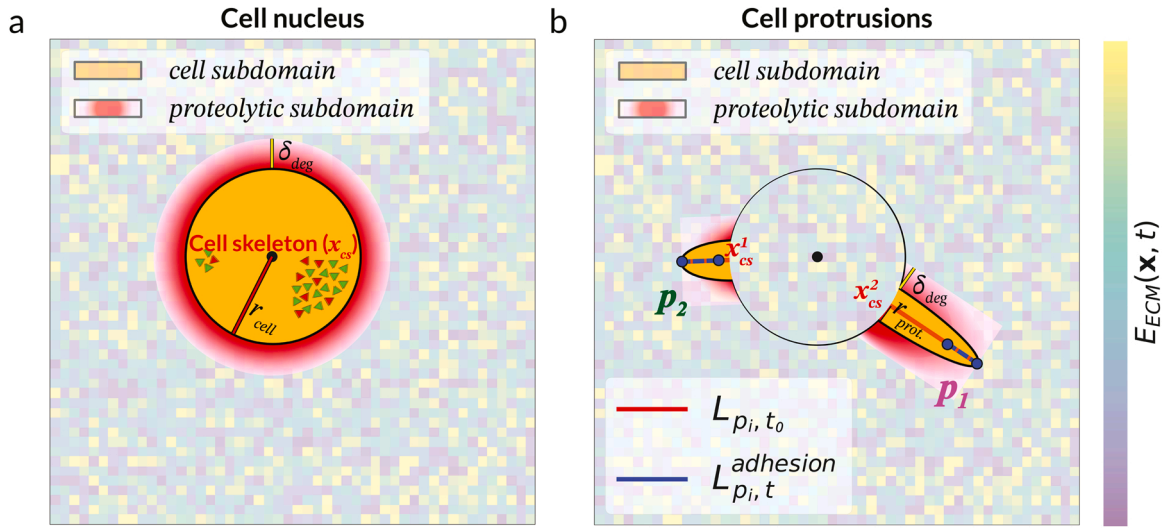

Fig. 6. Two-dimensional representation of the ECM degradation model. A cell with two protrusions (p_1 and p_2) in which the center of the cell body is represented by a black circle. The protrusions' adhesive regions were depicted as blue dashes lines, and their boundaries as blue circles. The ECM was discretized and each squared region had an associated stiffness ($E_{ECM}(x, t)$), represented as a colored square in the background. After a time interval, the ECM subdomain occupied by the cell ($d(x, x_{cs}) \leq r_{cell}$ in (**a**) and $d(x, x_{cs}) \leq r_{prot.}$ in (**b**), in orange) would have a very low associated stiffness. For locations x closer to the central region of the cell, $r = r_{cell}$ (**a**). For these locations, the proteolytic subdomain around the plasma membrane (PM) where MMPs are located and cleaving the ECM fibrilar network is delimited by $r' = r_{cell} + \delta_{deg}$. Conversely, locations x closer to one of cell's protrusions, $r = r_{prot.}$ (**b**). In this case, the proteolytic subdomain surrounding the PM where MMP degradation activity occurs is delimited by $r' = r_{prot.} + \delta_{deg}$. These proteolytic subdomains were colored as red gradients. Note that the protrusion adhesive region does not degrade its surrounding microenvironment.

displacements of the nodes during the expansive and contractile stages.

2.7. Numerical implementation

This model was implemented in Python using powerful libraries such as NumPy (Harris et al., 2020), SciPy (Virtanen et al., 2020), and Scikit-learn (Pedregosa et al., 2011) to maximize the performance of the model.

Following Merino-Casallo and colleagues (2018), we simulated the stochastic time evolution of this signaling network with the tau-leaping algorithm (Cao et al., 2006; Gillespie, 2001). This algorithm offers a good enough [5] approximation (Cazzaniga et al., 2006; Lok, 2004) of the exact solution given by the Stochastic Simulation Algorithm (SSA, also known as the Gillespie algorithm (Gillespie, 1977, 1976)).

We computed the displacements of the cell nucleus and protrusive structures using the Direct Stiffness Method. Mechanical equations were numerically solved.

We modeled the ECM as a 3D matrix of voxels with 2 μm edges. As the cell migrate within the surrounding ECM, it modifies the stiffness of voxels that it occupies. Cells also reduce the stiffness of those regions close enough to be affected by cellular proteolytic activity, which degrades ECM fibers. Therefore, this proteolytic mechanism required to update the stiffness of up to hundreds of thousands of voxels per iteration. Consequently, the algorithm implementing this mechanism took advantage of the efficient management of arrays of NumPy based on masks. To efficiently compute the distances from all those voxels to the cell skeleton, we used the k-dimensional trees (k-d trees) of Scikit-learn, which allows for k-nearest neighbors queries. We used experimental measurements from Valero and colleagues (2018) regarding the averaged ECM stiffness with respect to the matrix collagen concentration to initialize this 3D matrix representing the stiffness of the different ECM subdomains. Afterward, we could compute the averaged stiffness of any ROI at time t. We selected 10-μm radius spherical elements to manage ROIs as we considered them wide enough based on the protrusions' cross section (3.5 μm), the size of their adhesive region (≤ 8 μm), and their averaged length when cultured in collagen-based hydrogels (20 μm-30 μm).

The simulation of the chemosensing mechanism was decoupled from the cell-matrix interactive mechanism as we were considering two different time scales (Movilla et al., 2019; Merino-Casallo et al., 2018; Ribeiro et al., 2017). Indeed, the chemical and physical phenomena occur at different time scales. To accurately simulate the proposed signaling network, we used the iterative tau-leaping algorithm with a variable time step of 0.5–1.5 s. Nevertheless, to model the cell-matrix interactive mechanism, we used a different time step of 5 min. Besides, signal differences between two consecutive time steps were modest. In contrast, protrusions required more noticeable variations of the chemical signal to change their current state. As a result, we had to keep track of these cumulative variations in the chemical signal.

See Fig. 7 for a global scheme of the proposed mathematical model of 3D cell migration.

2.8. Example of application

In this work, we developed a computational model able to simulate mesenchymal-like migration within 3D matrices under different collagen concentrations and, consequently, distinct mechanical conditions. To evaluate the predictive potential of this *in silico* model, we replicated some previous *in vitro* experiments (Del Amo et al., 2017). In particular, we simulated the experiments evaluating cellular behavior in response to hydrogels with different collagen concentrations, which consequently present distinct architectural properties (e.g., stiffness, porosity, pore size). In those experiments, Del Amo and colleagues seeded NHDF cells in a 3D collagen matrix under step concentration gradients (Fig. 8).

[5] The "good-enough" phrase describing the accuracy of the tau-leaping algorithm comes from previous works such as Lok (2004) in which the author states that "One acceleration strategy is to abandon absolute mathematical precision in favor of a good-enough approximation. Gillespie has also been a pioneer in this effort. One of his strategies is called 'tau-leaping'." This statement is considered valid provided that the leap condition is satisfied, i.e., if the probability of each reaction taking place does not change significantly over the time leap.

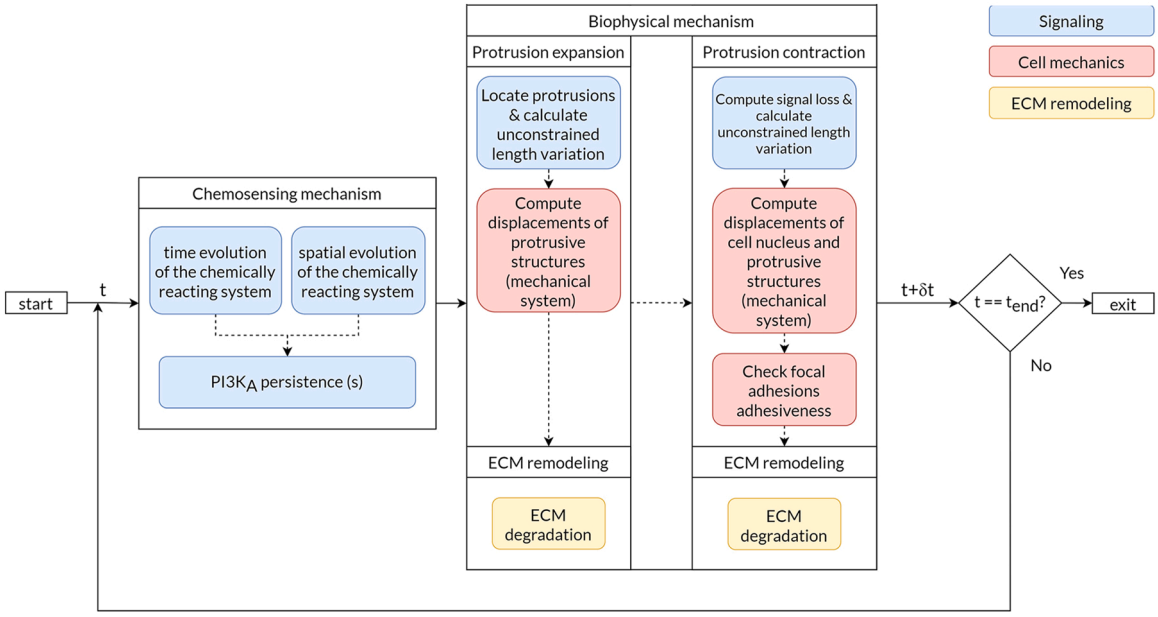

Fig. 7. Global scheme of the proposed mathematical model of 3D cell migration. Every iteration of the main algorithm started by simulating the spatiotemporal evolution of the simplified signaling network associated to the chemosensing mechanism. The expansive stage began by determining protrusions locations and their stress-free (unconstrained) length variation based on the $PI3K_A$ persistence. Then, we computed the displacements of each protrusive structure of the defined mechanical system. This second stage finished updating the stiffness of the ECM subdomain surrounding the cell. The last stage of the main algorithm (i.e., the contractile one), started by computing the signal loss because of protrusions contraction and time wear at those locations. Next, we computed the displacements of the cell nucleus and each protrusive structure because of protrusions contraction. Afterward, we updated the stiffness of the ECM subdomain surrounding the cell. If we had already arrived at the end of the simulation (t_{end}), the algorithm finished. Otherwise, we began a new iteration of the main algorithm.

The authors used microfluidic chips with three symmetric and adjacent channels. As a result, they could tweak the mechanical properties of each channel separately. In particular, we were interested in those *in vitro* assays where each channel had a different stiffness (Figure 8): (i) assay with single-step gradient hydrogels, and collagen concentrations of 1.5 mg ml^{-1} (39.78 Pa), 2.0 mg ml^{-1} (119.56 Pa), and 2.5 mg ml^{-1} (185.18 Pa), respectively (single assay); and (ii) assay with double-step gradient hydrogels, and collagen concentrations of 2.0 mg ml^{-1} (119.56 Pa), 1.5 mg ml^{-1} (39.78 Pa), and 4.0 mg ml^{-1} (360.67 Pa), respectively (*double assay*). Thus, there was a stiffness interface between channels. Note that the mechanical interface between channels 1 and 2 in both assays are equivalent, but with collagen densities (and ECM stiffnesses) exchanged. Their results showed that, in the absence of chemical gradients, collagen concentration and mechanical interfaces did not bias the distribution of NHDF cells toward stiffer regions during the individual invasion experiment.

We assumed that voxels associated with each channel of the microfluidic device, which may contain a specific collagen concentration, initially present a fixed stiffness. For instance, all voxels associated with a channel containing a 1.5 mg ml^{-1} collagen concentration would initially present a 39.78 Pa stiffness.

To avoid unrealistic scenarios, we started by calibrating the parameters mainly associated with protrusion dynamics, that is, those mainly regulating protrusion number (E_{p_i}, s_{binary}, s_{birth}, s_{growth}, and s_{death}), length (α_{gr} and β_{gr}), and migration speeds (c). We took advantage of the autonomous methodology proposed in Merino-Casallo et al. (2018) based on Bayesian optimization techniques to calibrate these parameters.

To calibrate the parameters mainly regulating the number of protrusions at each timepoint, we used previous experimental observations. Conversely, to calibrate the parameters primarily modulating protrusions length and speed of migration, we used experimental observations from (Merino-Casallo et al., 2018). However, this time we decided to use measurements from cells cultured in collagen-based hydrogels with different densities (2.0 mg ml^{-1} and 4.0 mg ml^{-1}). Consequently, we could consider how differences in matrix rigidity influence these features.

See Supplementary Section S4 for more details on the calibration of the parameters associated with protrusion dynamics.

3. Results

In this work, we were interested in how cells sense and respond to different biophysical cues, such as ECM stiffness and pore size. In the considered *in vitro* assays, this would mainly happen at the mechanical interfaces between two channels. When cells get close enough to these mechanical interfaces, they may extend protrusions toward both sides, which would allow them to attach to the different matrices and sense their biophysical differences. By initially locating cells in the different mechanical interfaces (i.e., in the interface between two channels, yellow lines in Fig. 8) in our simulations, we focused on this phenomenon, right from the beginning. Thus, we considered that simulating the first 24 hours of those *in vitro* assays, instead of the full 8 days, were enough for our specific interests.

We simulated the different scenarios (*single assay* and *double assay*, n = 20) described in Section 2.8 using the base parametrization (Supplementary Table S2 and Supplementary Table S3), not only considering the nuclear and/or adhesive phenotypes but also inhibiting or enabling ECM degradation.

We started by investigating the predicted migratory response of the proposed *in silico* model when dismissing both the adhesive and nuclear phenotypes and inhibiting ECM degradation. Note that, during their migration, cells create channel-like tracks within the surrounding environment with very low ECM stiffness, even when ECM degradation is inhibited. In this case, simulated cells exhibited a clear durotactic response toward stiffer environments (i.e., positive durotaxis; Fig. 9).

Next, we studied how the adhesive and nuclear phenotypes modulated, on their own, the predicted migratory response.

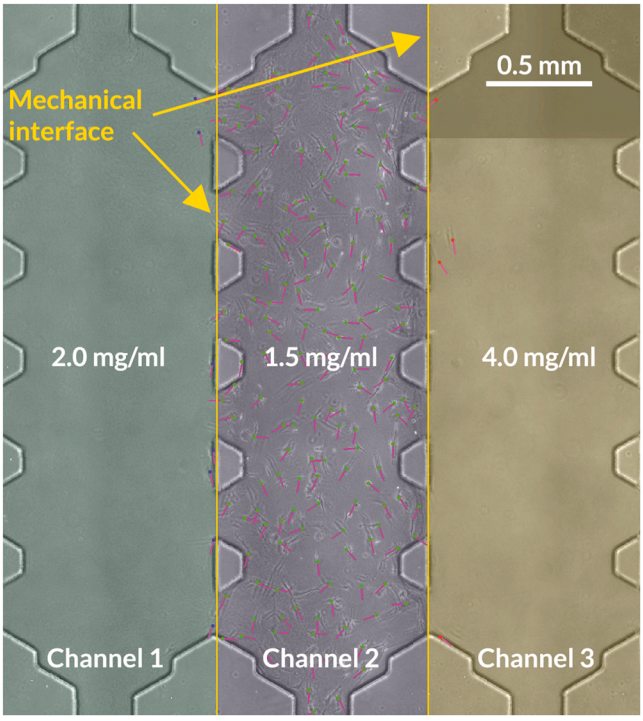

Fig. 8. Initial distribution of Norman Human Dermal Fibroblast (NHDF) cultured in a microfluidic device with three different channels. Each channel may include collagen-based gels at different concentrations of collagen (e.g., 2.0 μmg ml^{-1} in bottle green, 1.5 μmg ml^{-1} in eggplant, and 4.0 μmg ml^{-1} in mustard, respectively). Therefore, their associated stiffness may differ (e.g., 119.56 Pa in bottle green, 39.78 Pa in eggplant, and 360.67 Pa in mustard, respectively). Yellow lines represent the channel boundaries (corresponding to collagen interfaces). Green dots represent centroids of cells located in the central channel. Conversely, the blue and red dots represent centroids of cells located in the lateral channels. Purple straight lines represent cell orientation. Images were captured with a Nikon D-Eclipse Microscope with a Plan Fluor 10x Objective.
(Adapted from Del Amo and colleagues (2017)).

3.1. Adhesive and nuclear phenotypes modulate cells' migratory response

The adhesive phenotype, defined by parameters R_{min} and R_{max}, could predict different migratory behaviors. Some pairs of values for these parameters allowed the proposed *in silico* model to predict extreme cases such as a complete positive (Figure S2) or negative durotaxis (Figure S3). Intermediate cases emerged with other values for R_{min} and R_{max} (Figure S4 and Figure S5), where cells exhibit an adurotactic behavior in one of the mechanical interfaces simulated. Nevertheless, we could not find a single pair of values for R_{min} and R_{max} allowing the proposed *in silico* model to predict an adurotactic response for every mechanical interface simulated.

We found a similar trend if the model considered just the nuclear phenotype. The model could predict a positive durotaxis for *in silico* cells initially located in each mechanical interface (Figure S6). A different set of values would allow the model to predict an adurotactic response for cells in the mechanical interface between channels 1 and 2 for both assays (Figure S7) or in the mechanical interface between channels 2 and 3 (Figure S8). We also found some set of values resulting in a negative durotaxis for cells in specific mechanical interfaces such as the one between channels 2 and 3 for the double assay (Figure S9). Nonetheless, we could not find a set of values for the corresponding parameters ($E_{ECM}^{no\ \ eff}$, E_{ECM}^{arrest}, and γ^{fr}) enabling this model to predict an adurotactic response in every mechanical interface simulated.

Only by considering cells adhesive and nuclear phenotypes at the same time, we could find a set of parameters that enabled the proposed *in silico* model to predict this adurotactic response in every mechanical interface simulated (Figure 10). However, this was only possible if we considered a nonlinear response to the increasing constricting effect of the matrix steric hindrance ($\gamma^{fr} = 0.75$). The mechanical interface between channels 1 and 2 in both assays are equivalent, but with collagen densities (and ECM stiffnesses) exchanged. Therefore, differences regarding cell distribution and trajectories between both assays in this particular mechanical interface should probably be associated with the stochastic nature of the proposed *in silico* model.

Together, these results highlight the impact of both the adhesive and nuclear phenotypes on cell's migratory response when cultured in 3D environments.

3.2. ECM degradation promotes positive durotaxis in dense environments

To investigate the impact of ECM degradation in cell migration within 3D environments, we used the base parametrization (Supplementary Table S2 and Supplementary Table S3), considering an adhesive phenotype defined by $R_{min} = 9.46 \times 10^2$ pN and $R_{max} = 1.25$ pN, and a nuclear phenotype defined by $E_{ECM}^{no\ \ eff} = 16$ Pa, $E_{ECM}^{arrest} = 390$ Pa, and $\gamma^{fr} = 0.75$, which predicted an adurotactic behavior in every mechanical interface simulated when ECM degradation was inhibited (Figure 9). In addition, we tested the effect of different degradation rates (α_{deg}; 1.46×10^{-6} s^{-1} and 1.46×10^{-5} s^{-1}), which would translate on different speeds of matrix degradation. Enabling ECM degradation resulted on a reduction of the ECM stiffness sensed by cells (Figure S11a). Nevertheless, distinct ECM degradation rates did not translate in notable differences on the surrounding stiffness sensed by cells in general (Figure s11b).

A lower ECM degradation rate ($\alpha_{deg} = 1.46 \times 10^{-6}$ s^{-1}) resulted on cells significantly changing their migratory response just in the mechanical interface between channels 2 and channel 3 of the *double assay*, which contained collagen-based hydrogels at 1.5 mg ml^{-1} (39.78 Pa) and at 4.0 mg ml^{-1} (360.67 Pa), respectively (Fig. 11). Conversely, a higher ECM degradation rate ($\alpha_{deg} = 1.46 \times 10^{-5}$ s^{-1}) promoted cells positive durotaxis for those located at the mechanical interface between channel 2 and channel 3 of the double assay and also of the single assay, which contained collagen-based hydrogels at 2.0 mg ml^{-1} (119.56 Pa) and at 2.5 mg ml^{-1} (185.18 Pa), respectively (Fig. 12).

Together, these results highlight the impact of small local heterogeneities in ECM stiffness on cell's migratory response.

4. Discussion and conclusions

The proposed model builds upon an intracellular signaling network and focuses on cell-matrix interactions. These two building blocks have a leading role in 3D cell migration (Li et al., 2020; Krause et al., 2019; Yamada and Sixt, 2019). In this model, the local stiffness of the surrounding microenvironment modulates cell mechanics, namely, the growth and retraction of cell protrusions, as well as the cell nucleus translocation. The diameter of cells' nuclei and its deformability can hinder cells' ability to squeeze their nuclei through ECM pores (Wang et al., 2018; Wolf et al., 2013). Consequently, we investigated the influence of the nuclear phenotype. We also considered cell's adhesive phenotype by including an approximation to the clutch model. As a result, protrusions' adhesion to the ECM depended on their exerted contractile forces (Elosegui-Artola et al., 2018). Lastly, we studied the impact of cells' ability to degrade the surrounding matrix. Matrix stiffness and confinement impacts cell migration in 3D microenvironments, with the ECM acting as a physical barrier (Janmey et al., 2020; Malik et al., 2020; Zanotelli et al., 2020). ECM degradation dynamically changes the mechanical properties of the surrounding environment, decreasing its stiffness and level of confinement, and enables cells to create space around themselves.

In our previous works (Merino-Casallo et al., 2018; Ribeiro et al.,

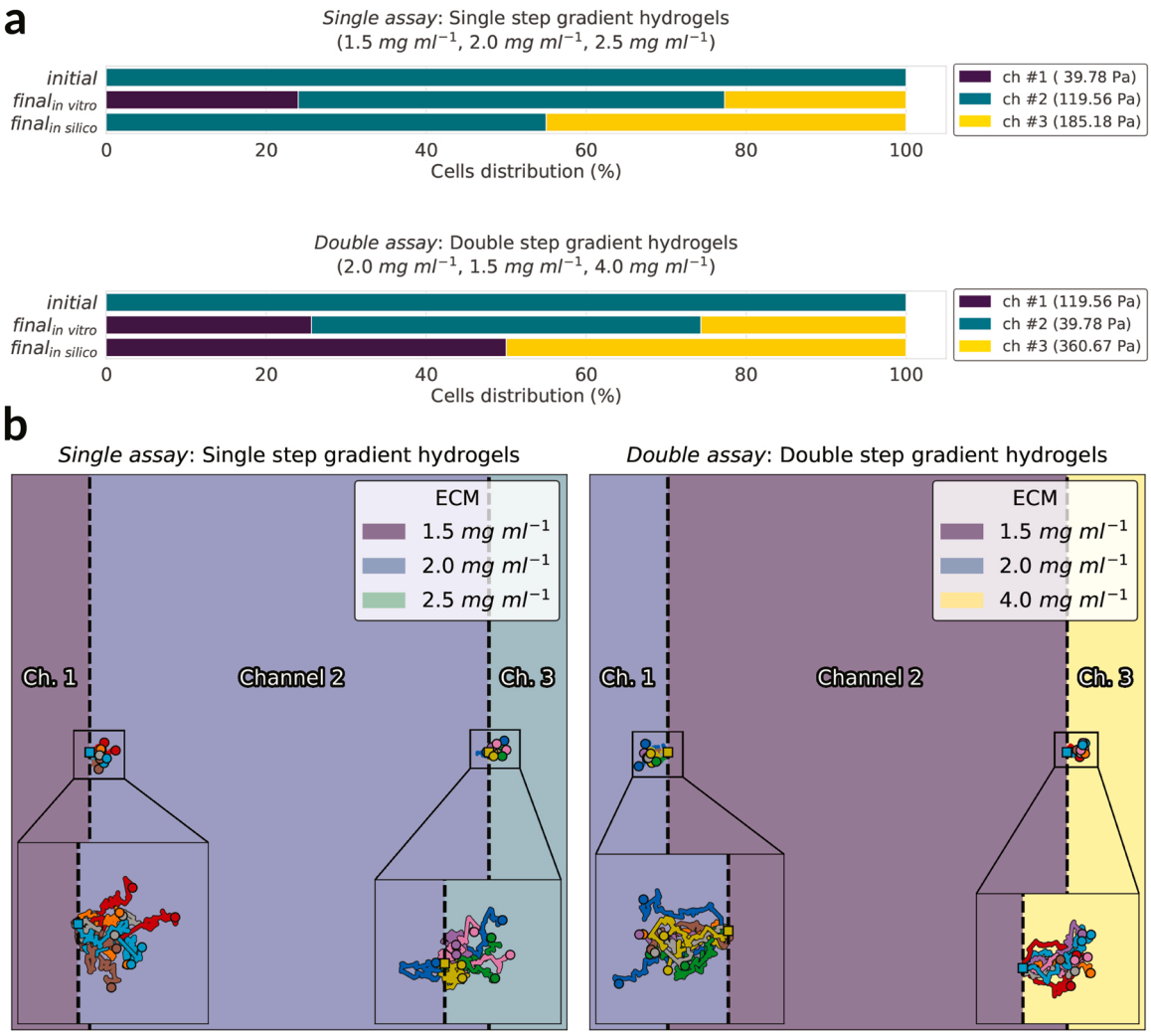

Fig. 9. **a**: Cells distribution for the *single assay* (**top**) and the *double assay* (**bottom**) from Del Amo and colleagues (2017), where cells were cultured in a microfluidic device with three channels, for the *in vitro* model ($n \in [50, 100]$), and the *in silico* model ($n = 20$). **b**: Cells trajectories for the *single assay* (**left**) and the *double assay* (**right**) from Del Amo and colleagues (2017), for the *in silico* model proposed in this work ($n = 20$). Cells' starting position is represented by squares whereas their final location is marked with circles. The medium in each channel had different physical properties corresponding with different concentrations of collagen. In the *single assay*, collagen concentrations were 1.5 mg ml^{-1}, 2.0 mg ml^{-1}, and 2.5 mg ml^{-1}, respectively, with single step gradient hydrogels. Therefore, the associated stiffnesses would be 39.78 Pa, 119.56 Pa, and 185.18 Pa, respectively. In the double assay, collagen concentrations were 2.0 mg ml^{-1}, 1.5 mg ml^{-1}, and 4.0 mg ml^{-1}, respectively, with double step gradient hydrogels. Hence, the associated stiffnesses would be 119.56 Pa, 39.78 Pa, and 360.67 Pa, respectively. We run simulations for 24 hours, with cells initially located at the interface between channels, using the base parametrization (Supplementary Table S2 and Supplementary Table S3), dismissing both the adhesive and nuclear phenotypes, and inhibiting ECM degradation.

2017), we considered protrusions analogous to an elastic inclusion (ellipsoid) embedded in the ECM and applied Eshelby's theory. We also assumed that the ECM was a continuous and homogeneous domain. Conversely, here we introduced a new approximation to physically model how protrusions expand, contract, and retract based on deformable bars and springs. Additionally, we modeled the ECM as a heterogeneous entity. Furthermore, we included matrix degradation, which is considered a relevant factor in 3D cell migration.

It is worth mentioning that Kim and colleagues (2018) proposed an *in silico* model with shared features. For one, their computational model considered the ECM as a heterogeneous entity too. Furthermore, the authors modeled how cells integrate mechanical stimuli and how these external cues influence cell migration within 3D matrices. They also modeled matrix degradation by cellular proteolytic activity. Nonetheless, there are remarkable differences between their work and ours. First and foremost, Kim and colleagues (2018) replicated experimental observations on flat surfaces where cells durotaxed (Lo et al., 2000). They did not consider factors that—although not relevant for migration on 2D substrates—play a significant role in motility in 3D scenarios. For example, they dismissed the influence of the steric hindrance of the ECM during cell motion, which may result in the surrounding matrix acting as a physical barrier. Also, the complexity of their model, and therefore its computational requirements, greatly exceeds ours.

Cells change their mode of migration based on the physical and chemical properties of the surrounding ECM (Yamada and Sixt, 2019). Carey and colleagues (2017) reported that 3D type I collagen substrates promoted mesenchymal gene expression and an MT1-MMP-dependent invasive epithelial phenotype. Interestingly, this phenotype was sensitive to the architecture and mechanics of collagen-based matrices. In contrast, culture in 3D basement membrane (Matrigel) did not induce such a cellular response. More recently, Janmey and colleagues (2020) also remarked that cells can also change their stiffness based on the stiffness of the ECM they are embedded in.

This *in silico* model considered that cell (cortical) stiffness is associated with the rigidity of the surrounding environment, as suggested by independent works (Rianna and Radmacher, 2017; Liu et al., 2013;

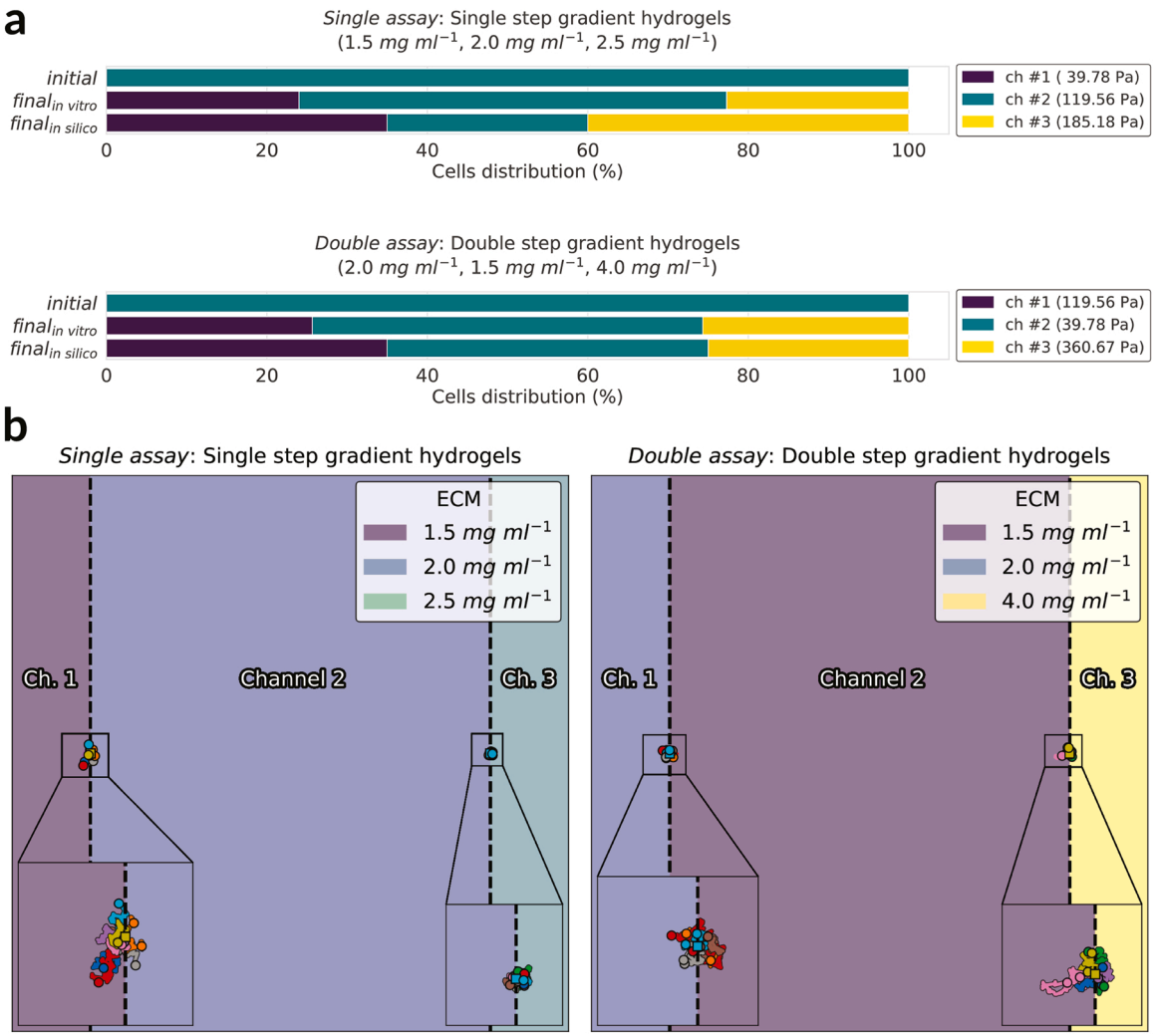

Fig. 10. **a**: Cells distribution for the *single assay* (**top**) and the *double assay* (**bottom**) from Del Amo and colleagues (2017), where cells were cultured in a microfluidic device with three channels, for the *in vitro* model ($n \in [50, 100]$), and the *in silico* model ($n = 20$). **b**: Cells trajectories for the *single assay* (**left**) and the *double assay* (**right**) from Del Amo and colleagues (2017), for the *in silico* model proposed in this work ($n = 20$). Cells' starting position is represented by squares whereas their final location is marked with circles. The medium in each channel had different physical properties corresponding with different concentrations of collagen. In the *single assay*, collagen concentrations were 1.5 mg ml^{-1}, 2.0 mg ml^{-1}, and 2.5 mg ml^{-1}, respectively, with single step gradient hydrogels. Therefore, the associated stiffnesses would be 39.78 Pa, 119.56 Pa, and 185.18 Pa, respectively. In the *double assay*, collagen concentrations were 2.0 mg ml^{-1}, 1.5 mg ml^{-1}, and 4.0 mg ml^{-1}, respectively, with double step gradient hydrogels. Hence, the associated stiffnesses would be 119.56 Pa, 39.78 Pa, and 360.67 Pa, respectively. We run simulations for 24 hours, with cells initially located at the interface between channels, using the base parametrization (Supplementary Table S2 and Supplementary Table S3), considering an adhesive phenotype defined by $R_{min} = 9.46 \times 10^{-2}$ pN and $R_{max} = 1.25$ pN, a nuclear phenotype defined by $E_{ECM}^{no\ \ eff} = 16$ Pa, $E_{ECM}^{arrest} = 390$ Pa, and $\gamma^{fr} = 0.75$, and inhibiting ECM degradation.

Chopra et al., 2011; Tee et al., 2011; Solon et al., 2007). However, a more recent study suggests that this long-established belief may be wrong (Rheinlaender et al., 2020). Thus, future experimental works should try to confirm this new hypothesis, and prospective theoretical and computational studies should consider this novel insight.

Changes in membrane tension trigger diverse cellular responses to modulate cell surface area (Le Roux et al., 2019; Thottacherry et al., 2018). For example, cells form and flatten PM folds to regulate membrane tension. As a result, cells are continuously remodeling their PM. However, the *in silico* model proposed in this work considered the cell membrane of the cell's central region containing its nucleus as the surface of a sphere with a fixed radius. Consequently, the volume of this central region was fixed at 4.91 mm^3. Protrusions, on the other hand, were considered tube-like geometries with a fixed cross-section but variable length. Therefore, the volume of the cell is not constant throughout our simulations. Indeed, as protrusions onset, grow, contract, and end up disappearing, their volume dynamically changes (around 3.85×10^{-7} mm^3–3.85×10^{-5} mm^3 per time step). Still, we assumed this as a valid approximation for our purposes. Note that other authors did consider cell shape deformations (Moure and Gomez, 2021; Winkler et al., 2019) at the cost of increasing the complexity of the proposed *in silico* models.

In this work, we focused on the architectural properties of the surrounding matrix, which are initially established based on the ECM collagen concentration. Features such as ECM porosity and the pore size of the matrix are related to collagen concentration as matrices with high collagen concentrations exhibit narrow pores (Zanotelli et al., 2022; Olivares et al., 2019; Fraley et al., 2015). This was phenomenologically included in the proposed *in silico* model through the $E_{ECM}^{no\ \ eff}$, E_{ECM}^{arrest}, and γ^{fr} parameters, which are associated with the cell's nuclear phenotype. These features are linked to the inability of some cell types to migrate efficiently in dense microenvironments (Li et al., 2020). Matrix porosity is also modified during tumorigenesis by both ECM synthesis and secretion, and matrix-remodeling enzymes (Zanotelli et al., 2020).

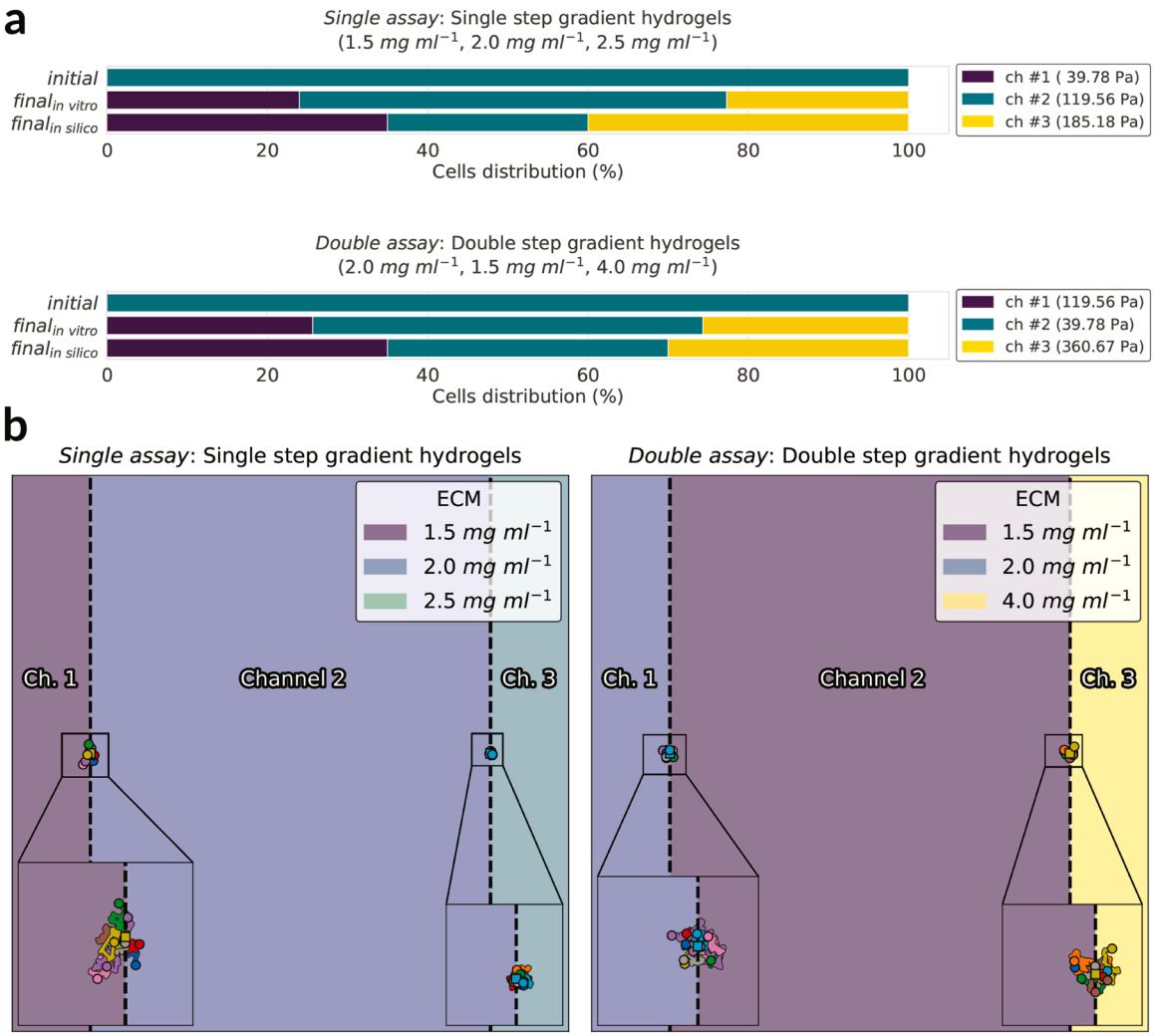

Fig. 11. **a**: Cells distribution for the *single assay* (**top**) and the *double assay* (**bottom**) from Del Amo and colleagues (2017), where cells were cultured in a microfluidic device with three channels, for the *in vitro* model ($n \in [50, 100]$), and the *in silico* model ($n = 20$). **b**: Cells trajectories for the *single assay* (**left**) and the *double assay* (**right**) from Del Amo and colleagues (2017), for the *in silico* model proposed in this work ($n = 20$). Cells' starting position is represented by squares whereas their final location is marked with circles. The medium in each channel had different physical properties corresponding with different concentrations of collagen. In the *single assay*, collagen concentrations were 1.5 mg ml^{-1}, 2.0 mg ml^{-1}, and 2.5 mg ml^{-1}, respectively, with single step gradient hydrogels. Therefore, the associated stiffnesses would be 39.78 Pa, 119.56 Pa, and 185.18 Pa, respectively. In the double assay, collagen concentrations were 2.0 mg ml^{-1}, 1.5 mg ml^{-1}, and 4.0 mg ml^{-1}, respectively, with double step gradient hydrogels. Hence, the associated stiffnesses would be 119.56 Pa, 39.78 Pa, and 360.67 Pa, respectively. We run simulations for 24 hours, with cells initially located at the interface between channels, using the base parametrization (Supplementary Table S2 and Supplementary Table S3), considering an adhesive phenotype defined by $R_{min} = 9.46 \times 10^2$ pN and $R_{max} = 1.25$ pN, a nuclear phenotype defined by $E_{ECM}^{no\ \ eff} = 16$ Pa, $E_{ECM}^{arrest} = 390$ Pa, and $\gamma^{fr} = 0.75$, and ECM degradation defined by $\alpha_{deg} = 1.46 \times 10^{-6}$ s^{-1} and $\delta_{deg} = 8.9 \times 10^{-3}$ mm. Cells exhibited a small increase in their tendency to migrate toward the stiffer environment when located in the mechanical interface between collagen-based hydrogels at 1.5 mg ml^{-1} (39.78 Pa) and 4.0 mg ml^{-1} (360.67 Pa) in the *double assay*.

Consequently, future studies should further investigate how ECM porosity and the pore size of the matrix influence the migratory process.

The proposed model did not consider fiber alignment, which has been reported as a critical enabler of cancer dissemination (Ray et al., 2017; Han et al., 2016). We assumed an isotropic distribution in each voxel of the 3D matrix representing the ECM. However, cells' ability to remodel the surrounding ECM also affects fiber alignment (Li et al., 2020). Janmey and colleagues (2020) recently noted that aligned fiber networks have also been suggested to be stiffer than unaligned matrix fibers. Therefore, further work is certainly required to study how dynamic changes in the alignment of fibers by cells during their migration affect their migratory patterns.

The presented model assumed a fixed ECM subdomain around the cell PM where the MMPs proteolytic activity occurs (defined by δ_{deg}). We considered this a valid assumption because we focused on migratory cells that do not stay at the same location during long periods. Future works may consider establishing a dynamic proteolytic subdomain and analyze how this change impacts cell behavior.

In 2D domains, cells can migrate toward the stiffer part of the substrate (a phenomenon known as durotaxis) (Sunyer et al., 2016; Lo et al., 2000). However, this durotactic behavior seems optimal within a given range of rigidities (Bangasser et al., 2017; Trichet et al., 2012). Besides, as other authors pointed out (Escribano et al., 2018; Janmey et al., 2020), factors such as pore size, porosity, fiber alignment, and matrix degradation regulate migration in 3D microenvironments (Huang et al., 2019; Liu et al., 2016; Wang et al., 2019)—even though they are not present or have a lower impact in 2D migration. Indeed, several authors have reported that 3D migration is impaired by the steric hindrance of the ECM (Cóndor et al., 2019; Movilla et al., 2018).

Cell response seems to depend on cell type and physiological or

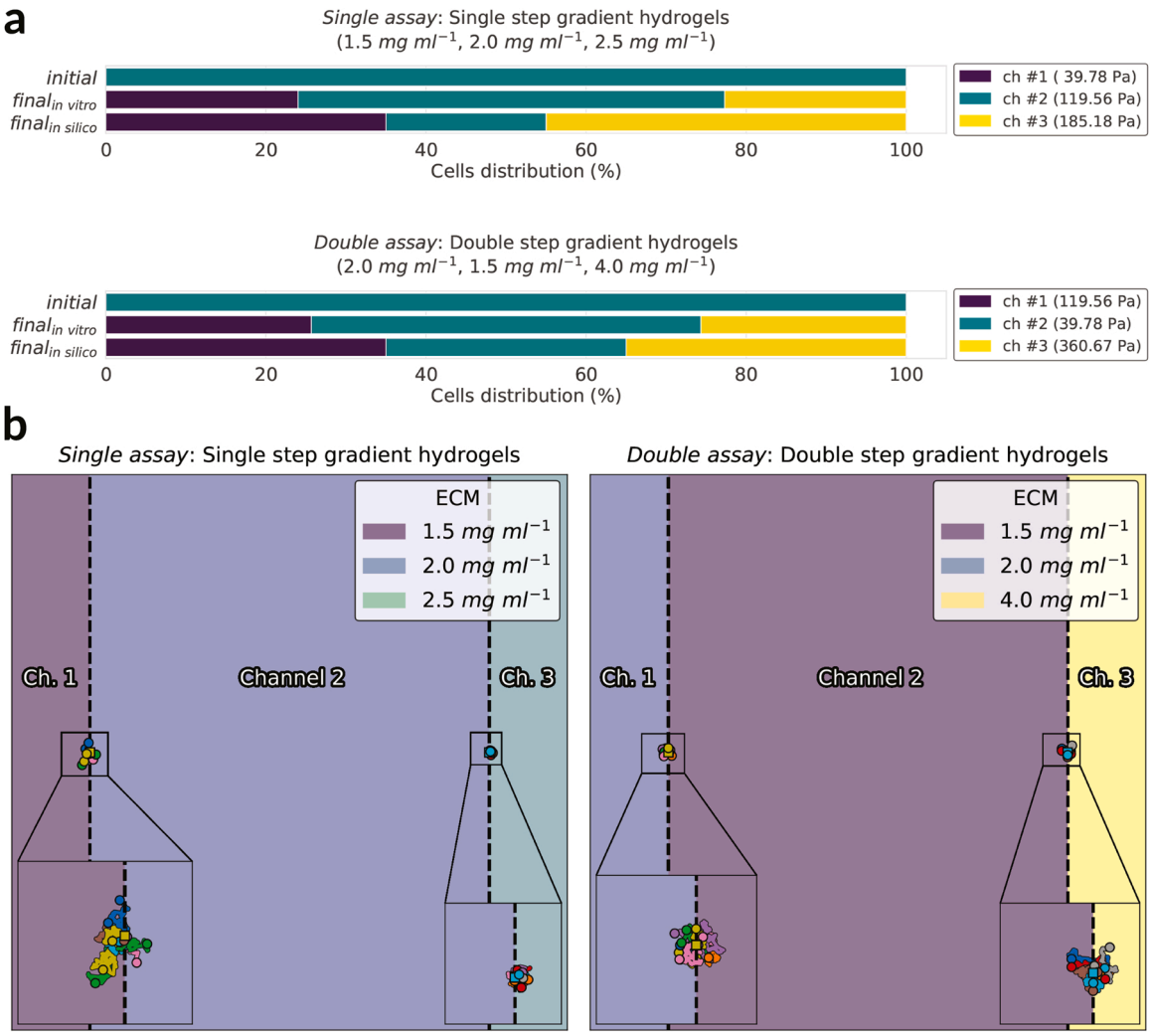

Fig. 12. **a**: Cells distribution for the *single assay* (**top**) and the *double assay* (**bottom**) from Del Amo and colleagues (2017), where cells were cultured in a microfluidic device with three channels, for the *in vitro* model ($n \in [50, 100]$), and the *in silico* model ($n = 20$). **b**: Cells trajectories for the *single assay* (**left**) and the *double assay* (**right**) from Del Amo and colleagues (2017), for the *in silico* model proposed in this work ($n = 20$). Cells' starting position is represented by squares whereas their final location is marked with circles. The medium in each channel had different physical properties corresponding with different concentrations of collagen. In the *single assay*, collagen concentrations were 1.5 mg ml^{-1}, 2.0 mg ml^{-1}, and 2.5 mg ml^{-1}, respectively, with single step gradient hydrogels. Therefore, the associated stiffnesses would be 39.78 Pa, 119.56 Pa, and 185.18 Pa, respectively. In the double assay, collagen concentrations were 2.0 mg ml^{-1}, 1.5 mg ml^{-1}, and 4.0 mg ml^{-1}, respectively, with double step gradient hydrogels. Hence, the associated stiffnesses would be 119.56 Pa, 39.78 Pa, and 360.67 Pa, respectively. We run simulations for 24 hours, with cells initially located at the interface between channels, using the base parametrization (Supplementary Table S2 and Supplementary Table S3), considering an adhesive phenotype defined by $R_{min} = 9.46 \times 10^2$ pN and $R_{max} = 1.25$ pN, a nuclear phenotype defined by $E_{ECM}^{no\ eff} = 16$ Pa, $E_{ECM}^{arrest} = 390$ Pa, and $\gamma^{fr} = 0.75$, and ECM degradation defined by $\alpha_{deg} = 1.46 \times 10^{-5}$ s^{-1} and $\delta_{deg} = 8.9 \times 10^{-3}$ mm. Cells exhibited a small increase in their tendency to migrate toward the stiffer environment when located in the mechanical interface between collagen-based hydrogels at both 2.0 mg ml^{-1} (119.56 Pa) and 2.5 mg ml^{-1} (185.18 Pa) in the single assay, and 1.5 mg ml^{-1} (39.78;Pa) and 4.0 mg ml^{-1} (360.67 Pa) in the *double assay*.

pathological conditions (Janmey et al., 2020). For instance, Shellard and Mayor (2021) recently showed for the first time that durotaxis does occur *in vivo*. Indeed, the neural crest of *Xenopus laevis* follows a self-generated stiffness gradient in the adjacent placodal tissue. Nonetheless, in some scenarios, cells may struggle to squeeze their nuclei through the surrounding ECM pores because of the nuclei diameter and rigidity or the size of these pores, which may even result in a complete migration arrest (McGregor et al., 2016). Isomursu and colleagues (2020) investigated cell preferential movements toward their stiffness optimum for maximal force transmission. Interestingly, preliminary reports from the authors suggest that there may be specific scenarios where cells would exhibit an antidurotactic response, that is, migration toward environments with lower ECM stiffness.

The proposed model was able to replicate some of the observations associated with *in vitro* experiments of NHDF embedded in collagen-based matrices, in which durotaxis does not occur. The prediction of an adurotactic response, similar to a random walk where ECM stiffness does not bias migration, only emerged when considering both the adhesive and nuclear phenotypes. Considering cells' nuclear phenotype through a friction term (μ) enabled us to simulate the ECM as a physical barrier in dense 3D environments (McGregor et al., 2016; Wolf et al., 2013), hindering the positive durotaxis that dominates on flat surfaces. The adhesive phenotype allowed us to replicate how cell-matrix adhesions are engaged only under optimal forces. If contractile forces transmitted to the ECM through these adhesive complexes are too low or too high, these bonds do not last long. Cells exhibiting a different adhesive phenotype (e.g., weakly adherent vs strongly adherent cells) may respond differently to ECM stiffness (Yeoman et al., 2021). If the proposed *in silico* model dismissed both the adhesive and nuclear phenotypes, it always predicted positive durotaxis. Only when considering

both phenotypes, our model could replicate the experimental observations from Del Amo and colleagues (2017). This model also highlighted the relevance of ECM degradation in cell migration within dense environments. Indeed, it enabled cells to create much needed space when migrating in confined matrices. As a result, cells may exhibit positive durotaxis in scenarios that otherwise would drive an adurotactic response or even negative durotaxis.

Overall, the proposed model replicates some of the main hallmarks of mesenchymal-like migration within 3D matrices. This model also highlights the relevance of the context in which cell motion is happening, that is, the cell phenotype and both the distinctive properties of the surrounding environment and its local heterogeneities. Therefore, we consider the presented *in silico* model a valuable tool to further investigate cell's migratory response in specific, complex, and more physiologically relevant 3D settings.

Funding

This work was supported by grants BES-2016–076291 (awarded to F. M.-C.), RTI2018–094494-B-C21 (awarded to J.M.G.-A. and M.J.G.-B.), PID2021-124271OB-I00 (awarded to M.J.G.-B.) and RTI2018–096903-B-I00 (awarded to to R.M.-C.) from the Spanish Ministry of Science and Innovation (MCIN/AEI/10.13039/501100011033),M and partially financed by the European Union through ERDF A way of making Europe; the Department of Science, University and Knowledge of the Government of Aragon [T50_20R]; and the European Union through PRIMAGE (PRedictive In-silico Multiscale Analytics to support cancer personalized diaGnosis and prognosis, empowered by imaging biomarkers), a Horizon 2020 RIA project (Topic SC1-DTH-07–2018, grant agreement no: 826494). This work is also part of a project that has received funding from the European Research Council (ERC) under the European Union's Horizon 2020 research and innovation program (ICoMICS grant agreement no: 101018587).

CRediT authorship contribution statement

Francisco Merino-Casallo: Conceptualization, Formal analysis, Investigation, Methodology, Calibration, Visualization, Writing - original draft, Writing - review & editing. **Maria Jose Gomez-Benito:** Conceptualization, Formal analysis, Methodology, Funding acquisition, Project administration, Supervision, Writing - review & editing. **Ruben Martinez-Cantin:** Calibration, Writing - review & editing. **Jose Manuel Garcia-Aznar:** Conceptualization, Formal analysis, Funding acquisition, Project administration, Supervision, Writing - review & editing.

Acknowledgments

We thank S. Perez-Rodriguez, and Y. Juste-Lanas for sharing with us their experimental data. We are also grateful for the insightful discussion and comments of F. Spill and the members of the M2BE. In particular, to C. Borau, D. Sainz-de-Mena, G. Nasello, N. Movilla, and S. Hervas-Raluy. Authors would also like to acknowledge the use of Servicio General de Apoyo a la Investigación-SAI, Universidad de Zaragoza.

Appendix A. Supporting information

Supplementary data associated with this article can be found in the online version at doi:10.1016/j.ejcb.2022.151255.

References

Addison, W., 1842. Experimental and practical researches on the nature and origin of tubercles in the lungs. Prov. Med. Surg. J. 1–4, 403–407. https://doi.org/10.1136/bmj.s1-4.20.403.

Alert, R., Trepat, X., 2020. Physical models of collective cell migration. Annu. Rev. Condens. Matter Phys. 11, 77–101. https://doi.org/10.1146/annurev-conmatphys-031218-013516.

Bangasser, B.L., Shamsan, G.A., Chan, C.E., Opoku, K.N., Tüzel, E., Schlichtmann, B.W., Kasim, J.A., Fuller, B.J., McCullough, B.R., Rosenfeld, S.S., Odde, D.J., 2017. Shifting the optimal stiffness for cell migration. Nat. Commun. 8, 15313 https://doi.org/10.1038/ncomms15313.

Bentley, K., Mariggi, G., Gerhardt, H., Bates, P.A., 2009. Tipping the balance: robustness of tip cell selection, migration and fusion in angiogenesis. PLOS Comput. Biol. 5, e1000549 https://doi.org/10.1371/journal.pcbi.1000549.

Beunk, L., Bakker, G.J., van Ens, D., Bugter, J., Gal, F., Svoren, M., Friedl, P., Wolf, K., 2022. Actomyosin contractility requirements and reciprocal cell-tissue mechanics for cancer cell invasion through collagen-based channels. Eur. Phys. J. E 45, 1–14. https://doi.org/10.1140/EPJE/S10189-022-00182-6.

Borau, C., Kamm, R.D., García-Aznar, J.M., 2011. Mechano-sensing and cell migration: a 3D model approach. Phys. Biol. 8, 66008–66013. https://doi.org/10.1088/1478-3975/8/6/066008.

Buttenschön, A., Edelstein-Keshet, L., 2020. Bridging from single to collective cell migration: a review of models and links to experiments. PLOS Comput. Biol. 16, e1008411 https://doi.org/10.1371/journal.pcbi.1008411 arXiv:2011.10873.

Calero-Cuenca, F.J., Janota, C.S., Gomes, E.R., 2018. Dealing with the nucleus during cell migration. Curr. Opin. Cell Biol. 50, 35–41. https://doi.org/10.1016/J.CEB.2018.01.014.

Camley, B.A., Rappel, W.J., 2017. Physical models of collective cell motility: from cell to tissue. J. Phys. D. Appl. Phys. 50, 113002 https://doi.org/10.1088/1361-6463/aa56fe.

Campbell, E.J., Bagchi, P., 2017. A computational model of amoeboid cell swimming. Phys. Fluids 29, 101902. https://doi.org/10.1063/1.4990543.

Campbell, E.J., Bagchi, P., 2020. A computational study of amoeboid motility in 3D: the role of extracellular matrix geometry, cell deformability, and cell-matrix adhesion. Biomech. Model. Mechanobiol. 1–25. https://doi.org/10.1007/s10237-020-01376-7.

Cao, Y., Gillespie, D.T., Petzold, L.R., 2006. Efficient step size selection for the tau-leaping simulation method. J. Chem. Phys. 124, 044109 https://doi.org/10.1063/1.2159468.

Carey, S.P., Martin, K.E., Reinhart-King, C.A., 2017. Three-dimensional collagen matrix induces a mechanosensitive invasive epithelial phenotype. Sci. Rep. 7, 42088 https://doi.org/10.1038/srep42088.

Caswell, P.T., Zech, T., 2018. Actin-based cell protrusion in a 3D matrix. Trends Cell Biol. 28, 823–834. https://doi.org/10.1016/J.TCB.2018.06.003.

Caton, R., 1870. Contributions to the cell-migration theory. J. Anat. Physiol. 5, 35–420, 7.

Cazzaniga, P., Pescini, D., Besozzi, D., Mauri, G., 2006. Tau leaping stochastic simulation method in P systems. In: Proceedings of the Int. Work. Membr. Comput. Springer, Berlin, Heidelberg, pp. 298–313. https://doi.org/10.1007/11963516_19 (pp).

Chiu, C.L., Aguilar, J.S., Tsai, C.Y., Wu, G., Gratton, E., Digman, M.A., 2014. Nanoimaging of focal adhesion dynamics in 3D. PLOS One 9, e99896. https://doi.org/10.1371/journal.pone.0099896.

Chopra, A., Tabdanov, E., Patel, H., Janmey, P.A., Kresh, J.Y., 2011. Cardiac myocyte remodeling mediated by N-cadherin-dependent mechanosensing. Am. J. Physiol. Circ. Physiol. 300, 1252–1266. https://doi.org/10.1152/AJPHEART.00515.2010.

Cóndor, M., Mark, C., Gerum, R.C., Grummel, N.C., Bauer, A., García-Aznar, J.M., Fabry, B., 2019. Breast cancer cells adapt contractile forces to overcome steric hindrance. Biophys. J. 116, 1305–1312. https://doi.org/10.1016/j.bpj.2019.02.029.

Conway, J.R., Jacquemet, G., 2019. Cell matrix adhesion in cell migration. Essays Biochem. 63, 535–551. https://doi.org/10.1042/EBC20190012.

Daub, J.T., Merks, R.M.H., 2013. A cell-based model of extracellular-matrix-guided endothelial cell migration during angiogenesis. Bull. Math. Biol. 75, 1377–1399. https://doi.org/10.1007/s11538-013-9826-5.

De Pascalis, C., Etienne-Manneville, S., 2017. Single and collective cell migration: the mechanics of adhesions. Mol. Biol. Cell 28, 1833–1846. https://doi.org/10.1091/mbc.E17-03-0134.

Del Amo, C., Borau, C., Movilla, N., Asín, J., García-Aznar, J.M., 2017. Quantifying 3D chemotaxis in microfluidic-based chips with step gradients of collagen hydrogel concentrations. Integr. Biol. 9, 339–349. https://doi.org/10.1039/C7IB00022G.

Doyle, A.D., Sykora, D.J., Pacheco, G.G., Kutys, M.L., Yamada, K.M., 2021. 3D mesenchymal cell migration is driven by anterior cellular contraction that generates an extracellular matrix prestrain. Dev. Cell 56 (6), 826–841.e4.. https://doi.org/10.1016/j.devcel.2021.02.017.

Elosegui-Artola, A., Trepat, X., Roca-Cusachs, P., 2018. Control of mechanotransduction by molecular clutch dynamics. Trends Cell Biol. 28, 356–367. https://doi.org/10.1016/j.tcb.2018.01.008.

Escribano, J., Sunyer, R., Sánchez, M.T., Trepat, X., Roca-Cusachs, P., García-Aznar, J.M., 2018. A hybrid computational model for collective cell durotaxis. Biomech. Model. Mechanobiol. 17, 1–16. https://doi.org/10.1007/s10237-018-1010-2.

Escribano, J., Chen, M.B., Moeendarbary, E., Cao, X., Shenoy, V., Garcia-Aznar, J.M., Kamm, R.D., Spill, F., 2019. Balance of mechanical forces drives endothelial gap formation and may facilitate cancer and immune-cell extravasation. PLOS Comput. Biol. 15, e1006395 https://doi.org/10.1371/journal.pcbi.1006395.

Fang, Y., Gong, H., Yang, R., Lai, K.W., Quan, M., 2020. An active biomechanical model of cell adhesion actuated by intracellular tensioning-taxis. Biophys. J. 118, 2656–2669. https://doi.org/10.1016/j.bpj.2020.04.016.

Faraj, K.A., Van Kuppevelt, T.H., Daamen, W.F., 2007. Construction of collagen scaffolds that mimic the three-dimensional architecture of specific tissues. Tissue Eng. 13, 2387–2394. https://doi.org/10.1089/ten.2006.0320.

Fischer, T., Hayn, A., Mierke, C.T., 2020. Effect of nuclear stiffness on cell mechanics and migration of human breast cancer cells. Front. Cell Dev. Biol. 8, 393. https://doi.org/10.3389/FCELL.2020.00393/BIBTEX.

Fraley, S.I., Wu, P.h.H., He, L., Feng, Y., Krisnamurthy, R., Longmore, G.D., Wirtz, D., 2015. Three-dimensional matrix fiber alignment modulates cell migration and MT1-MMP utility by spatially and temporally directing protrusions. Sci. Rep. 5, 14580. https://doi.org/10.1038/srep14580.

Friedl, P., Mayor, R., 2017. Tuning collective cell migration by cell-cell junction regulation. Cold Spring Harb. Perspect. Biol. 9, a029199 https://doi.org/10.1101/cshperspect.a029199.

Gillespie, D.T., 1976. A general method for numerically simulating the stochastic time evolution of coupled chemical reactions. J. Comput. Phys. 22, 403–434. https://doi.org/10.1016/0021-9991(76)90041-3.

Gillespie, D.T., 1977. Exact stochastic simulation of coupled chemical reactions. J. Phys. Chem. 81, 2340–2361. https://doi.org/10.1021/j100540a008.

Gillespie, D.T., 2001. Approximate accelerated stochastic simulation of chemically reacting systems. J. Chem. Phys. 115, 1716–1733. https://doi.org/10.1063/1.1378322.

Gonzalez-Valverde, I., Garcia-Aznar, J.M., 2018. Mechanical modeling of collective cell migration: an agent-based and continuum material approach. Comput. Methods Appl. Mech. Eng. 337, 246–262. https://doi.org/10.1016/j.cma.2018.03.036.

Guimarães, C.F., Gasperini, L., Marques, A.P., Reis, R.L., 2020. The stiffness of living tissues and its implications for tissue engineering. Nat. Rev. Mater. 5, 351–370. https://doi.org/10.1038/s41578-019-0169-1.

Haeger, A., Wolf, K., Zegers, M.M., Friedl, P., 2015. Collective cell migration: guidance principles and hierarchies. Trends Cell Biol. 25, 556–566. https://doi.org/10.1016/j.tcb.2015.06.003.

Han, W., Chen, S., Yuan, W., Fan, Q., Tian, J., Wang, X., Chen, L., Zhang, X., Wei, W., Liu, R., Qu, J., Jiao, Y., Austin, R.H., Liu, L., 2016. Oriented collagen fibers direct tumor cell intravasation. Proc. Natl. Acad. Sci. USA 113. https://doi.org/10.1073/pnas.1610347113.

Harris, C.R., Millman, K.J., van der Walt, S.J., Gommers, R., Virtanen, P., Cournapeau, D., Wieser, E., Taylor, J., Berg, S., Smith, N.J., Kern, R., Picus, M., Hoyer, S., van Kerkwijk, M.H., Brett, M., Haldane, A., del Rio, J.F., Wiebe, M., Peterson, P., Gerard-Marchant, P., Sheppard, K., Reddy, T., Weckesser, W., Abbasi, H., Gohlke, C., Oliphant, T.E., 2020. Array programming with NumPy. Nature 585, 357–362. https://doi.org/10.1038/s41586-020-2649-2.

Hatakeyama, M., Kimura, S., Naka, T., Kawasaki, T., Yumoto, N., Ichikawa, M., Kim, J. H., Saito, K., Saeki, M., Shirouzu, M., Yokoyama, S., Konagaya, A., 2003. A computational model on the modulation of mitogen-activated protein kinase (MAPK) and Akt pathways in heregulin-induced ErbB signalling. Biochem. J. 373, 451–463. https://doi.org/10.1042/BJ20021824.

Hayn, A., Fischer, T., Mierke, C.T., 2020. Inhomogeneities in 3D collagen matrices impact matrix mechanics and cancer cell migration. Front. Cell Dev. Biol. 8, 1224. https://doi.org/10.3389/fcell.2020.593879.

Heck, T., Vargas, D.A., Smeets, B., Ramon, H., van Liedekerke, P., van Oosterwyck, H., 2020. The role of actin protrusion dynamics in cell migration through a degradable viscoelastic extracellular matrix: Insights from a computational model. PLOS Comput. Biol. 16, e1007250 https://doi.org/10.1371/journal.pcbi.1007250.

Hervas-Raluy, S., Garcia-Aznar, J.M., Gomez-Benito, M.J., 2019. Modelling actin polymerization: the effect on confined cell migration. Biomech. Model. Mechanobiol. 18, 1177–1187. https://doi.org/10.1007/s10237-019-01136-2.

Hoehme, S., Drasdo, D., 2010. A cell-based simulation software for multi-cellular systems. Bioinformatics 26, 2641–2642. https://doi.org/10.1093/bioinformatics/btq437.

Huang, D., Nakamura, Y., Ogata, A., Kidoaki, S., 2019. Characterization of 3D matrix conditions for cancer cell migration with elasticity/porosity-independent tunable microfiber gels. Polym. J. 52, 333–344. https://doi.org/10.1038/s41428-019-0283-3.

Insall, R., 2021. Actin in 2021. Curr. Biol. 31, R496–R498. https://doi.org/10.1016/j.cub.2021.04.013.

Isomursu, A., Park, K.-Y., Hou, J., Cheng, B., Shamsan, G., Fuller, B., Kasim, J., Mohsen Mahmoodi, M., Lu, T.J., Genin, G.M., Xu, F., Lin, M., Distefano, M., Ivaska, J., Odde, D.J., 2020. Negative durotaxis: cell movement toward softer environments. bioRxiv Prepr. https://doi.org/10.1101/2020.10.27.357178.

Janmey, P.A., Fletcher, D.A., Reinhart-King, C.A., 2020. Stiffness sensing by cells. Physiol. Rev. 100, 695–724. https://doi.org/10.1152/physrev.00013.2019.

Kechagia, J.Z., Ivaska, J., Roca-Cusachs, P., 2019. Integrins as biomechanical sensors of the microenvironment. Nat. Rev. Mol. Cell Biol. 20, 457–473. https://doi.org/10.1038/s41580-019-0134-2.

Kelkar, M., Bohec, P., Charras, G., 2020. Mechanics of the cellular actin cortex: from signalling to shape change. Curr. Opin. Cell Biol. 66, 69–78. https://doi.org/10.1016/j.ceb.2020.05.008 arXiv:2005.11854.

Kim, M.C., Silberberg, Y.R., Abeyaratne, R., Kamm, R.D., Asada, H.H., 2018. Computational modeling of three-dimensional ECM-rigidity sensing to guide directed cell migration. Proc. Natl. Acad. Sci. USA 115, E390–E399. https://doi.org/10.1073/pnas.1717230115.

Krause, M., Wolf, K., 2015. Cancer cell migration in 3D tissue: negotiating space by proteolysis and nuclear deformability. Cell Adhes. Migr. 9, 357–366. https://doi.org/10.1080/19336918.2015.1061173.

Krause, M., Yang, F.W., te Lindert, M., Isermann, P., Schepens, J., Maas, R.J.A., Venkataraman, C., Lammerding, J., Madzvamuse, A., Hendriks, W., teRiet, J., Wolf, K., 2019. Cell migration through three-dimensional confining pores: speed accelerations by deformation and recoil of the nucleus. Philos. Trans. R. Soc. B Biol. Sci. 374, 20180225 https://doi.org/10.1098/rstb.2018.0225.

Le Roux, A.L., Quiroga, X., Walani, N., Arroyo, M., Roca-Cusachs, P., 2019. The plasma membrane as a mechanochemical transducer. Philos. Trans. R. Soc. B: Biol. Sci. 374 https://doi.org/10.1098/rstb.2018.0221.

Lee, S.W.L., Seager, R.J., Litvak, F., Spill, F., Sieow, J.L., Leong, P.H., Kumar, D., Tan, A. S.M., Wong, S.C., Adriani, G., Zaman, M.H., Kamm, R.D., 2020. Integrated *in silico* and 3D *in vitro* model of macrophage migration in response to physical and chemical factors in the tumor microenvironment. Integr. Biol. 12, 90–108. https://doi.org/10.1093/INTBIO/ZYAA007.

Lehtimaki, J., Hakala, M., Lappalainen, P., 2017. Actin filament structures in migrating cells. Handb. Exp. Pharmacol. 235, 1–30. https://doi.org/10.1007/164_2016_28.

Letort, G., Montagud, A., Stoll, G., Heiland, R., Barillot, E., MacKlin, P., Zinovyev, A., Calzone, L., 2019. PhysiBoSS: a multi-scale agent-based modelling framework integrating physical dimension and cell signalling. Bioinformatics 35, 1188–1196. https://doi.org/10.1093/bioinformatics/bty766.

Li, A., Sun, M., Spill, F., Sun, R., Zaman, M.H., 2019. Are the effects of independent biophysical factors linearly additive? A 3D tumor migration model. Biophys. J. 117, 1702–1713. https://doi.org/10.1016/J.BPJ.2019.09.037.

Li, J., Jung, W., Nam, S., Chaudhuri, O., Kim, T., 2020. Roles of interactions between cells and extracellular matrices for cell migration and matrix remodeling. In: Proceedings of the Multi-scale Extracell. Matrix Mech. Mechanobiol. Springer, pp. 247–282. https://doi.org/10.1007/978-3-030-20182-1_8 (pp).

Lim, F.Y., Koon, Y.L., Chiam, K.H., 2013. A computational model of amoeboid cell migration. Comput. Methods Biomech. Biomed. Eng. 16, 1085–1095. https://doi.org/10.1080/10255842.2012.757598.

Lintz, M., Muñoz, A., Reinhart-King, C.A., 2017. The mechanics of single cell and collective migration of tumor cells. J. Biomech. Eng. 139, 9. https://doi.org/10.1115/1.4035121.

Liu, H., Sun, Y., Simmons, C.A., 2013. Determination of local and global elastic moduli of valve interstitial cells cultured on soft substrates. J. Biomech. 46, 1967–1971. https://doi.org/10.1016/J.JBIOMECH.2013.05.001.

Liu, L., Luo, Q., Sun, J., Song, G., 2016. Nucleus and nucleus-cytoskeleton connections in 3D cell migration. Exp. Cell Res. 348, 56–65. https://doi.org/10.1016/J.YEXCR.2016.09.001.

Lo, C.M., Wang, H.B., Dembo, M., Wang, Y.L., 2000. Cell movement is guided by the rigidity of the substrate. Biophys. J. 79, 144–152. https://doi.org/10.1016/S0006-3495(00)76279-5.

Lok, L., 2004. The need for speed in stochastic simulation. Nat. Biotechnol. 22, 964–965. https://doi.org/10.1038/nbt0804-964.

Mak, M., Spill, F., Kamm, R.D., Zaman, M.H., 2016. Single-cell migration in complex microenvironments: mechanics and signaling dynamics. J. Biomech. Eng. 138, 021004 https://doi.org/10.1115/1.4032188.

Malik, A.A., Wennberg, B., Gerlee, P., 2020. The impact of elastic deformations of the extracellular matrix on cell migration. Bull. Math. Biol. 82, 1–19. https://doi.org/10.1007/s11538-020-00721-2.

Marin-Riera, M., Brun-Usan, M., Zimm, R., Välikangas, T., Salazar-Ciudad, I., 2016. Computational modeling of development by epithelia, mesenchyme and their interactions: a unified model. Bioinformatics 32, 219–225. https://doi.org/10.1093/bioinformatics/btv527.

Mason, D.E., Collins, J.M., Dawahare, J.H., Nguyen, T.D., Lin, Y., Voytik-Harbin, S.L., Zorlutuna, P., Yoder, M.C., Boerckel, J.D., 2019. YAP and TAZ limit cytoskeletal and focal adhesion maturation to enable persistent cell motility. J. Cell Biol. 218, 1369–1389. https://doi.org/10.1083/jcb.201806065.

McGregor, A.L., Hsia, C.R., Lammerding, J., 2016. Squish and squeeze – the nucleus as a physical barrier during migration in confined environments. Curr. Opin. Cell Biol. 40, 32–40. https://doi.org/10.1016/J.CEB.2016.01.011.

Merino-Casallo, F., Gomez-Benito, M.J., Juste-Lanas, Y., Martinez-Cantin, R., Garcia-Aznar, J.M., 2018. Integration of *in vitro* and *in silico* models using bayesian optimization with an application to stochastic modeling of mesenchymal 3D cell migration. Front. Physiol. 9, 1246. https://doi.org/10.3389/fphys.2018.01246.

Merino-Casallo, F., Gomez-Benito, M.J., Hervas-Raluy, S., Garcia-Aznar, J.M., 2022. Unravelling cell migration: defining movement from the cell surface. Cell Adhes. Migr. 16, 25–64. https://doi.org/10.1080/19336918.

Milde, F., Tauriello, G., Haberkern, H., Koumoutsakos, P., 2014. SEM++: a particle model of cellular growth, signaling and migration. Comput. Part. Mech. 1, 211–227. https://doi.org/10.1007/s40571-014-0017-4.

Moreira-Soares, M., Cunha, S.P., Bordin, J.R., Travasso, R.D., 2020. Adhesion modulates cell morphology and migration within dense fibrous networks. J. Phys. Condens. Matter 32, 314001. https://doi.org/10.1088/1361-648X/ab7c17.

Moure, A., Gomez, H., 2018. Three-dimensional simulation of obstacle-mediated chemotaxis. Biomech. Model. Mechanobiol. 17 https://doi.org/10.1007/s10237-018-1023-x.

Moure, A., Gomez, H., 2021. Phase-field modeling of individual and collective cell migration. Arch. Comput. Methods Eng. 28, 331–344. https://doi.org/10.1007/s11831-019-09377-1.

Movilla, N., 2021. Análisis del efecto de la matriz extracelular en la migración 3D de fibroblastos y osteoblastos humanos. / Nieves Movilla Meno. (Ph.D. thesis). University of Zaragoza.

Movilla, N., Borau, C., Valero, C., García-Aznar, J.M., 2018. Degradation of extracellular matrix regulates osteoblast migration: a microfluidic-based study. Bone 107, 10–17. https://doi.org/10.1016/j.bone.2017.10.025.

Movilla, N., Valero, C., Borau, C., García-Aznar, J.M., 2019. Matrix degradation regulates osteoblast protrusion dynamics and individual migration. Integr. Biol. 11, 404–413. https://doi.org/10.1093/intbio/zyz035.

Mukherjee, A., Barai, A., Singh, R.K., Yan, W., Sen, S., 2020. Nuclear plasticity increases susceptibility to damage during confined migration. PLOS Comput. Biol. 16, e1008300 https://doi.org/10.1371/journal.pcbi.1008300.

Nasello, G., Alaman-Diez, P., Schiavi, J., PerezAnson, M.A., McNamara, L.M., Garcia-Aznar, J.M., 2020. Primary human osteoblasts cultured in a 3D microenvironment

create a unique representative model of their differentiation into osteocytes. Front. Bioeng. Biotechnol. 8, 336. https://doi.org/10.3389/FBIOE.2020.00336.
Olivares, V., Cóndor, M., DelAmo, C., Asín, J., Borau, C., García-Aznar, J.M., 2019. Image-based characterization of 3D collagen networks and the effect of embedded cells. Microsc. Microanal. 25, 971–981. https://doi.org/10.1017/S1431927619014570.
Paul, C.D., Mistriotis, P., Konstantopoulos, K., 2017. Cancer cell motility: lessons from migration in confined spaces. Nat. Rev. Cancer 17, 131–140. https://doi.org/10.1038/nrc.2016.123.
Paul, C.D., Hruska, A., Staunton, J.R., Burr, H.A., Daly, K.M., Kim, J., Jiang, N., Tanner, K., 2019. Probing cellular response to topography in three dimensions. Biomaterials 197, 101–118. https://doi.org/10.1016/J.BIOMATERIALS.2019.01.009.
Pedregosa, F., Varoquaux, G., Gramfort, A., Michel, V., Thirion, B., Grisel, O., Blondel, M., Prettenhofer, P., Weiss, R., Dubourg, V., Vanderplas, J., Passos, A., Cournapeau, D., Brucher, M., Perrot, M., Duchesnay, É., 2011. Scikit-learn: machine learning in python. J. Mach. Learn. Res. 12, 2825–2830.
Pérez-Rodríguez, S., Tomás-González, E., García-Aznar, J., 2018. 3D cell migration studies for chemotaxis on microfluidic-based chips: a comparison between cardiac and dermal fibroblasts. Bioengineering 5, 45. https://doi.org/10.3390/bioengineering5020045.
Petrie, R.J., Doyle, A.D., Yamada, K.M., 2009. Random versus directionally persistent cell migration. Nat. Rev. Mol. Cell Biol. 10, 538–549. https://doi.org/10.1038/nrm2729.
Pfeffer, W., 1884.Locomotorische Richtungsbewegungen durch chemische Reize:(Aus den" Untersuchungen aus dem botanischen Institut zu Tübingen Bd. I. Heft 3 p. 363–482). W. Engelmann.
Ray, A., Slama, Z.M., Morford, R.K., Madden, S.A., Provenzano, P.P., 2017. Enhanced directional migration of cancer stem cells in 3D aligned collagen matrices. Biophys. J. 112, 1023–1036.
Rens, E.G., Merks, R.M., 2020. Cell shape and durotaxis explained from cell-extracellular matrix forces and focal adhesion dynamics. iScience 23, 101488. https://doi.org/10.1016/j.isci.2020.101488.
Rheinlaender, J., Dimitracopoulos, A., Wallmeyer, B., Kronenberg, N.M., Chalut, K.J., Gather, M.C., Betz, T., Charras, G., Franze, K., 2020. Cortical cell stiffness is independent of substrate mechanics. Nat. Mater. 19, 1019–1025. https://doi.org/10.1038/s41563-020-0684-x.
Rianna, C., Radmacher, M., 2017. Comparison of viscoelastic properties of cancer and normal thyroid cells on different stiffness substrates. Eur. Biophys. J. 46, 309–324. https://doi.org/10.1007/s00249-016-1168-4.
Ribeiro, F.O., Gómez-Benito, M.J., Folgado, J., Fernandes, P.R., García-Aznar, J.M., 2017. Computational model of mesenchymal migration in 3D under chemotaxis. Comput. Methods Biomech. Biomed. Eng. 20, 59–74. https://doi.org/10.1080/10255842.2016.1198784.
Ridley, A.J., Schwartz, M.A., Burridge, K., Firtel, R.A., Ginsberg, M.H., Borisy, G., Parsons, J.T., Horwitz, A.R., 2003. Cell migration: integrating signals from front to back. Science 302, 1704–1709. https://doi.org/10.1126/science.1092053.
Ringer, P., Colo, G., Fässler, R., Grashoff, C., 2017. Sensing the mechano-chemical properties of the extracellular matrix. Matrix Biol. 64, 6–16. https://doi.org/10.1016/J.MATBIO.2017.03.004.
Rubashkin, M.G., Cassereau, L., Bainer, R., DuFort, C.C., Yui, Y., Ou, G., Paszek, M.J., Davidson, M.W., Chen, Y.Y., Weaver, V.M., 2014. Force engages vinculin and promotes tumor progression by enhancing PI3K activation of phosphatidylinositol (3,4,5)-triphosphate. Cancer Res. 74, 4597–4611. https://doi.org/10.1158/0008-5472.CAN-13-3698.
Schlüter, D., Ramis-Conde, I., Chaplain, M., 2012. Computational modeling of single-cell migration: the leading role of extracellular matrix fibers. Biophys. J. 103, 1141–1151. https://doi.org/10.1016/J.BPJ.2012.07.048.
Scianna, M., Preziosi, L., Wolf, K., 2012. A cellular potts model simulating cell migration on and in matrix environments. Math. Biosci. Eng. 10, 235–261. https://doi.org/10.3934/mbe.2013.10.235.
SenGupta, S., Parent, C.A., Bear, J.E., 2021. The principles of directed cell migration. Nat. Rev. Mol. Cell Biol. 1–19. https://doi.org/10.1038/s41580-021-00366-6.
Senju, Y., Lappalainen, P., 2019. Regulation of actin dynamics by PI(4,5)P2 in cell migration and endocytosis. Curr. Opin. Cell Biol. 56, 7–13. https://doi.org/10.1016/J.CEB.2018.08.003.
Serrano-Alcalde, F., García-Aznar, J.M., Gómez-Benito, M.J., 2017. The role of nuclear mechanics in cell deformation under creeping flows. J. Theor. Biol. 432, 25–32. https://doi.org/10.1016/J.JTBI.2017.07.028.
Serrano-Alcalde, F., García-Aznar, J.M., Gómez-Benito, M.J., 2020. Cell biophysical stimuli in lobodopodium formation: a computer based approach. Comput. Methods Biomech. Biomed. Eng. 1–10. https://doi.org/10.1080/10255842.2020.1836622.
Shellard, A., Mayor, R., 2020. Rules of collective migration: from the wildebeest to the neural crest: Rules of neural crest migration. Philos. Trans. R. Soc. B Biol. Sci. 375 https://doi.org/10.1098/rstb.2019.0387.
Shellard, A., Mayor, R., 2021. Collective durotaxis along a self-generated stiffness gradient *in vivo*. Nature 600, 690–694. https://doi.org/10.1038/s41586-021-04210-x.
Singh, A., Nascimento, J.M., Kowar, S., Busch, H., Boerries, M., 2012. Boolean approach to signalling pathway modelling in HGF-induced keratinocyte migration. Bioinformatics 28, i495–i501. https://doi.org/10.1093/bioinformatics/bts410.
Solon, J., Levental, I., Sengupta, K., Georges, P.C., Janmey, P.A., 2007. Fibroblast adaptation and stiffness matching to soft elastic substrates. Biophys. J. 93, 4453–4461. https://doi.org/10.1529/BIOPHYSJ.106.101386.
Sun, M., Zaman, M.H.H., 2017. Modeling, signaling and cytoskeleton dynamics: integrated modeling-experimental frameworks in cell migration. Wiley Interdiscip. Rev. Syst. Biol. Med. 9, e1365 https://doi.org/10.1002/wsbm.1365.
Sun, Z., Costell, M., Fässler, R., 2019. Integrin activation by talin, kindlin and mechanical forces. Nat. Cell Biol. 21 https://doi.org/10.1038/s41556-018-0234-9.
Sunyer, R., Conte, V., Escribano, J., Elosegui-Artola, A., Labernadie, A., Valon, L., Navajas, D., García-Aznar, J.M., Muñoz, J.J., Roca-Cusachs, P., Trepat, X., 2016. Collective cell durotaxis emerges from long-range intercellular force transmission. Science 353, 1157–1161. https://doi.org/10.1126/science.aaf7119.
Svitkina, T., 2018. The actin cytoskeleton and actin-based motility. Cold Spring Harb. Perspect. Biol. 10 https://doi.org/10.1101/cshperspect.a018267.
Taufalele, P.V., VanderBurgh, J.A., Muñoz, A., Zanotelli, M.R., Reinhart-King, C.A., 2019. Fiber alignment drives changes in architectural and mechanical features in collagen matrices. PLOS One 14, e0216537. https://doi.org/10.1371/journal.pone.0216537.
Tee, S.Y., Fu, J., Chen, C.S., Janmey, P.A., 2011. Cell shape and substrate rigidity both regulate cell stiffness. Biophys. J. 100, L25–L27. https://doi.org/10.1016/J.BPJ.2010.12.3744.
Theocharis, A.D., Skandalis, S.S., Gialeli, C., Karamanos, N.K., 2016. Extracellular matrix structure. Adv. Drug Deliv. Rev. 97, 4–27. https://doi.org/10.1016/j.addr.2015.11.001.
Thottacherry, J.J., Kosmalska, A.J., Kumar, A., Vishen, A.S., Elosegui-Artola, A., Pradhan, S., Sharma, S., Singh, P.P., Guadamillas, M.C., Chaudhary, N., Vishwakarma, R., Trepat, X., del Pozo, M.A., Parton, R.G., Rao, M., Pullarkat, P., Roca-Cusachs, P., Mayor, S., 2018. Mechanochemical feedback control of dynamin independent endocytosis modulates membrane tension in adherent cells. Nat. Commun. 9, 1–14. https://doi.org/10.1038/s41467-018-06738-5.
Trichet, L., LeDigabel, J., Hawkins, R.J., Vedula, S.R.K., Gupta, M., Ribrault, C., Hersen, P., Voituriez, R., Ladoux, B., 2012. Evidence of a large-scale mechanosensing mechanism for cellular adaptation to substrate stiffness. Proc. Natl. Acad. Sci. USA 109, 6933–6938. https://doi.org/10.1073/pnas.1117810109.
Valero, C., Javierre, E., García-Aznar, J.M., Gómez-Benito, M.J., 2014. Nonlinear finite element simulations of injuries with free boundaries: application to surgical wounds. Int. J. Numer. Method. Biomed. Eng. 30, 616–633. https://doi.org/10.1002/cnm.2621.
Valero, C., Amaveda, H., Mora, M., García-Aznar, J.M., 2018. Combined experimental and computational characterization of crosslinked collagen-based hydrogels. PLOS One 13, e0195820. https://doi.org/10.1371/journal.pone.0195820.
Van Liedekerke, P., Palm, M.M., Jagiella, N., Drasdo, D., 2015. Simulating tissue mechanics with agent-based models: concepts, perspectives and some novel results. Comput. Part. Mech. 2, 401–444. https://doi.org/10.1007/s40571-015-0082-3.
Vargas, D.A., Gonçalves, I.G., Heck, T., Smeets, B., Lafuente-Gracia, L., Ramon, H., Van Oosterwyck, H., 2020. Modeling of mechanosensing mechanisms reveals distinct cell migration modes to emerge from combinations of substrate stiffness and adhesion receptor-ligand affinity. Front. Bioeng. Biotechnol. 8, 459. https://doi.org/10.3389/fbioe.2020.00459.
Vermolen, F.J., Javierre, E., 2012. A finite-element model for healing of cutaneous wounds combining contraction, angiogenesis and closure. J. Math. Biol. 65, 967–996. https://doi.org/10.1007/s00285-011-0487-4.
Virtanen, P., Gommers, R., Oliphant, T.E., Haberland, M., Reddy, T., Cournapeau, D., Burovski, E., Peterson, P., Weckesser, W., Bright, J., van der Walt, S.J., Brett, M., Wilson, J., Millman, K.J., Mayorov, N., Nelson, A.R., Jones, E., Kern, R., Larson, E., Carey, C.J., Polat, I., Feng, Y., Moore, E.W., VanderPlas, J., Laxalde, D., Perktold, J., Cimrman, R., Henriksen, I., Quintero, E.A., Harris, C.R., Archibald, A.M., Ribeiro, A.H., Pedregosa, F., van Mulbregt, P., Vijaykumar, A., Bardelli, A.P., Rothberg, A., Hilboll, A., Kloeckner, A., Scopatz, A., Lee, A., Rokem, A., Woods, C.N., Fulton, C., Masson, C., Häggström, C., Fitzgerald, C., Nicholson, D.A., Hagen, D.R., Pasechnik, D.V., Olivetti, E., Martin, E., Wieser, E., Silva, F., Lenders, F., Wilhelm, F., Young, G., Price, G.A., Ingold, G.L., Allen, G.E., Lee, G.R., Audren, H., Probst, I., Dietrich, J.P., Silterra, J., Webber, J.T., Slavič, J., Nothman, J., Buchner, J., Kulick, J., Schönberger, J.L., de Miranda Cardoso, J.V., Reimer, J., Harrington, J., Rodríguez, J.L.C., Nunez-Iglesias, J., Kuczynski, J., Tritz, K., Thoma, M., Newville, M., Kümmerer, M., Bolingbroke, M., Tartre, M., Pak, M., Smith, N.J., Nowaczyk, N., Shebanov, N., Pavlyk, O., Brodtkorb, P.A., Lee, P., McGibbon, R.T., Feldbauer, R., Lewis, S., Tygier, S., Sievert, S., Vigna, S., Peterson, S., More, S., Pudlik, T., Oshima, T., Pingel, T.J., Robitaille, T.P., Spura, T., Jones, T.R., Cera, T., Leslie, T., Zito, T., Krauss, T., Upadhyay, U., Halchenko, Y.O., Vázquez-Baeza, Y., 2020. SciPy 1.0: fundamental algorithms for scientific computing in Python. Nat. Methods 17, 261–272. https://doi.org/10.1038/s41592-019-0686-2 arXiv: 1907.10121.
Wang, P., Dreger, M., Madrazo, E., Williams, C.J., Samaniego, R., Hodson, N.W., Monroy, F., Baena, E., Sanchez-Mateos, P., Hurlstone, A., Redondo-Muñoz, J., 2018. WDR5 modulates cell motility and morphology and controls nuclear changes induced by a 3D environment. Proc. Natl. Acad. Sci. USA 115, 8581–8586. https://doi.org/10.1073/PNAS.1719405115/SUPPL_FILE/PNAS.1719405115.SM15.AVI.
Wang, W.Y., Davidson, C.D., Lin, D., Baker, B.M., 2019. Actomyosin contractility-dependent matrix stretch and recoil induces rapid cell migration. Nat. Commun. 10, 1186. https://doi.org/10.1038/s41467-019-09121-0.
Wang, Z., Birch, C.M., Sagotsky, J., Deisboeck, T.S., 2009. Cross-scale, cross-pathway evaluation using an agent-based non-small cell lung cancer model. Bioinformatics 25, 2389–2396. https://doi.org/10.1093/bioinformatics/btp416.
Weiger, M.C., Ahmed, S., Welf, E.S., Haugh, J.M., 2010. Directional persistence of cell migration coincides with stability of asymmetric intracellular signaling. Biophys. J. 98, 67–75. https://doi.org/10.1016/J.BPJ.2009.09.051.

Welf, E.S., Ahmed, S., Johnson, H.E., Melvin, A.T., Haugh, J.M., 2012. Migrating fibroblasts reorient directionality: by a metastable, PI3K-dependent mechanism. J. Cell Biol. 197, 105–114. https://doi.org/10.1083/jcb.201108152.

Winkler, B., Aranson, I.S., Ziebert, F., 2019. Confinement and substrate topography control cell migration in a 3D computational model. Commun. Phys. 2, 82. https://doi.org/10.1038/s42005-019-0185-x.

Wolf, K., Wu, Y.I., Liu, Y., Geiger, J., Tam, E., Overall, C., Stack, M.S., Friedl, P., 2007. Multi-step pericellular proteolysis controls the transition from individual to collective cancer cell invasion. Nat. Cell Biol. 9, 893–904. https://doi.org/10.1038/ncb1616.

Wolf, K., TeLindert, M., Krause, M., Alexander, S., TeRiet, J., Willis, A.L., Hoffman, R.M., Figdor, C.G., Weiss, S.J., Friedl, P., 2013. Physical limits of cell migration: control by ECM space and nuclear deformation and tuning by proteolysis and traction force. J. Cell Biol. 201, 1069–1084. https://doi.org/10.1083/jcb.201210152.

Wu, P.H., Gilkes, D.M., Wirtz, D., 2018. The biophysics of 3D cell migration. Annu. Rev. Biophys. 47, 549–567. https://doi.org/10.1146/annurev-biophys-070816-033854.

Yamada, K.M., Sixt, M., 2019. Mechanisms of 3D cell migration. Nat. Rev. Mol. Cell Biol. 20, 738–752. https://doi.org/10.1038/s41580-019-0172-9.

Yeoman, B., Shatkin, G., Beri, P., Banisadr, A., Katira, P., Engler, A.J., 2021. Adhesion strength and contractility enable metastatic cells to become adurotactic. Cell Rep. 34, 108816 https://doi.org/10.1016/j.celrep.2021.108816.

Zanotelli, M.R., Chada, N.C., Johnson, C.A., Reinhart-King, C.A., 2020. The physical microenvironment of tumors: characterization and clinical impact. Phys. Cancer 165–195. https://doi.org/10.1142/9789811223495_0008.

Zanotelli, M.R., Zhang, J., Ortiz, I., Wang, W., Chada, N.C., Reinhart-King, C.A., 2022. Highly motile cells are metabolically responsive to collagen density. Proc. Natl. Acad. Sci. USA 119. https://doi.org/10.1073/PNAS.2114672119.

Zheng, Y., Fan, Q., Eddy, C.Z., Wang, X., Sun, B., Ye, F., Jiao, Y., 2020. Modeling multicellular dynamics regulated by extracellular-matrix-mediated mechanical communication via active particles with polarized effective attraction. Phys. Rev. E 102, 052409. https://doi.org/10.1103/PhysRevE.102.052409.

Zhu, R., Liu, C., Gundersen, G.G., 2018. Nuclear positioning in migrating fibroblasts. Semin. Cell Dev. Biol. 82, 41–50. https://doi.org/10.1016/J.SEMCDB.2017.11.006.

Zmurchok, C., Collette, J., Rajagopal, V., Holmes, W.R., 2020. Membrane tension can enhance adaptation to maintain polarity of migrating cells. Biophys. J. 119, 1617–1629. https://doi.org/10.1016/j.bpj.2020.08.035.